Universität Stuttgart

INSTITUT FÜR MECHANIK

Acoustic Time-Domain Simulation with BEM and FEM

by Eduardo Vargas Millán

Master's Thesis

under the guidance of
Dr.-Ing. Michael Mayer (Robert Bosch GmbH)

Institut für Angewandte und Experimentelle Mechanik
Universität Stuttgart
o. Prof. Dr.-Ing. habil. L. Gaul
Dipl.-Ing. J. Herrmann

August 2011

Contents

1. Introduction

1.1. The problem

The Finite Element Method is a numerical procedure which is widely recognized in a variety of engineering fields, such as aeronautical, biomechanical, and automotive industries. Several modern FEM packages are available and include specific components such as thermal, electromagnetic, fluid, and structural working environments.

On the other hand, the boundary element method (BEM) is a numerical method that approximates solutions to boundary integral equations. Such equations provide a well defined formulation of boundary-value problems also in different branches of engineering, e.g. elasticity, plasticity, fracture mechanics, ground water flow, wave propagation and electromagnetic field problems. However, commercial softwares that are available with this method are rare and are not used as much as the FEM packages. The problem with BEM lies on the numerical solution of this method. The main issues are the non-symmetric, fully populated system of equations we get in collocation and the difficulties to treat inhomogeneous and non-linear problems due to the treatment of volume integrals that arise.

When it comes to acoustics, specifically to external problems in which the radiation is emitted into an infinite acoustic medium, the user has to pay closely attention to this two methods available, BEM and FEM. The most noticeable difference between these methods concerns the discretisation. In FEM the complete domain Ω has to be discretised, whereas in BEM discretisation is restricted to the boundary $\Gamma = \partial\Omega$ (see Figure 1.1). This can lead to time savings in this kind of problems.

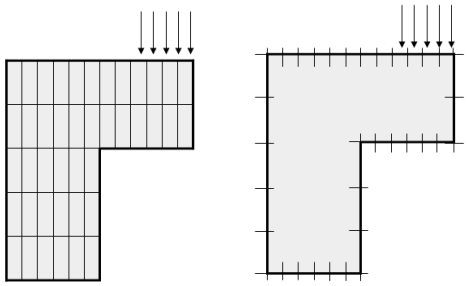

Figure 1.1.: Discretisation of a domain with finite elements (a) and boundary elements (b)

The time domain module of "*Virtual.Lab*" is a new release that is only available in the last version of this package and is lacking the theoretical background on its

manual. The objective of this investigation is to evaluate the utilization and liability of the boundary element software package "*Virtual.Lab*" in the time domain acoustic field by comparing the results with the finite element software package "*ABAQUS*", which has a proven background in acoustics and a well documented manual.

The body of the investigation is divided into chapters.

- The theoretical chapter gives a general overview of the theory needed to comprehend the investigation.
- In the next chapter, the approach taken to perform the evaluation is explained in detail.
- Then, the results and its analyses are contained in chapter III.
- and finally, concluding remarks and recommendations are summarized in the last chapter.

2. Theory and Principles

2.1. Basics in Acoustics

Acoustics is the science that deals with all mechanical waves in compressible continua including vibration, sound, ultrasound and infrasound. The audible frequency, in which we are interested, ranges from 16 Hz to 20000 Hz. In contrast to the different types of waves encountered in a solid body, only longitudinal waves appear in an inviscid fluid such as a perfect gas or a compressible liquid. An introduction to acoustic wave motion in fluids will be given in this section.

2.1.1. The Acoustic Wave Equation

The acoustic wave equation for the pressure field in a homogeneous, isotropic, and perfectly elastic fluid, neglecting dissipative effects, is derived from the continuity equation (2.1) and the conservation of momentum (2.2) according to *Gaul, Kögl and Wagner* [5].

$$\dot{\rho} + \rho \frac{\partial v_i}{\partial x_i} = 0, \tag{2.1}$$

$$\sigma_{ji,j} + \sigma b_i = \rho \dot{v}_i, \tag{2.2}$$

Assuming small density fluctuations $\bar{\rho}$ about the equilibrium density state ρ_0

$$\rho = \rho_0 + \bar{\rho} \quad with \quad \bar{\rho} \ll \rho_0, \tag{2.3}$$

we can linearize (2.1), so that we obtain

$$\dot{\bar{\rho}} + \rho_0 v_{i,i} = 0, \tag{2.4}$$

Since the fluid is inviscid, it does not transmit shear stresses and the stress tensor is given by

$$\sigma_{ij} = -p\delta_{ij}. \tag{2.5}$$

From (2.1) and neglecting body forces b_i, the local linearized balance of momentum is

$$\rho_0 \dot{v}_i = -p_{,i}. \tag{2.6}$$

Inserting the gradient of (2.6) into the material derivative of (2.4), we obtain

$$p_{,ii} - \ddot{\bar{\rho}} = 0. \tag{2.7}$$

Then selecting $\bar{\rho}$ as the independent state variable, we obtain the constitutive relation

$$\dot{p} = \frac{\partial p}{\partial \bar{\rho}} \dot{\bar{\rho}}, \tag{2.8}$$

which if inserted into (2.7), we obtain the *wave equation for the pressure field*

$$p_{,ii} - \frac{1}{c^2} \ddot{p} = 0, \tag{2.9}$$

where the acoustic wave velocity c depends on the material and is defined by

$$c := \sqrt{\frac{\partial p}{\partial \bar{\rho}}}. \tag{2.10}$$

The wave velocity equation (2.10) yields a constant if we perform a Taylor series about the equilibrium state up to the linear term and obtain the relation between the pressure fluctuations (or acoustic pressure) $\bar{p} = p - p_0$ and the density fluctuations $\bar{\rho}$

$$c := \sqrt{\left(\frac{\partial p}{\partial \rho}\right)_{\rho_o}}. \tag{2.11}$$

Another field variable that is commonly employed in acoustics is the *velocity potential* ϕ, which is defined as

$$v_i = -\phi_{,i}. \tag{2.12}$$

The wave equation for the velocity potential is analog to (2.9)

$$\phi_{,ii} - \frac{1}{c^2} \ddot{\phi} = 0. \tag{2.13}$$

2.1.2. Root mean square value

In general, the *effective value* $\tilde{y}$ of an arbitrary field quantity $y(t+T) = y(t)$ with the period time T is defined as

$$\tilde{y} = \sqrt{\frac{1}{T} \int_0^T y^2(t) dt}. \tag{2.14}$$

Now if $y(t)$ has a pure harmonic behavior with an amplitude $\hat{y}$, (2.14) yields

$$\tilde{y} = \frac{\hat{y}}{\sqrt{2}}. \tag{2.15}$$

2.1.3. Acoustic Impedance

The *specific acoustic impedance* is defined for harmonic fluctuations as

$$z(x) = \frac{p(x)}{v(x)}. \tag{2.16}$$

This ratio of complex numbers therefore directly quantifies the relative amplitude and phase of the pressure and particle velocity.

Planar, single-frequency traveling waves have acoustic impedance equal to the characteristic impedance.

$$Z_0 = \rho \cdot c. \tag{2.17}$$

2.1.4. Sound Intensity

Sound waves transport energy in the form of kinetic energy of particle motion and potential energy of elastic strain (fractional change of fluid volume). The measure of the magnitude and direction of the local rate of energy transport is termed the *sound intensity*: its symbol is I and its unit is W/m^2. Considering the time averaged acoustic intensity associated with spherical wave propagation. In three-dimensional harmonic wave propagation of period T, the intensity is given by

$$\mathbf{I} = \frac{1}{T} \int_{-T/2}^{T/2} p(t)\mathbf{v}(t)dt, \tag{2.18}$$

which is a vector quantity which depends both on the magnitude and the direction of the velocity vector $\mathbf{v}$.

2.1.5. Sound Power

The total power output P of a source is given by integrating the intensity traveling across a surface which totally encloses the source. The sound power output unit is W and is defined by

$$P = \int_S \mathbf{I} \cdot \mathbf{n} dS, \tag{2.19}$$

where $\mathbf{n}$ is the unit normal vector pointing outwards from the closed surface S

2.1.6. Structure-Borne Sound

Many acoustics events, such as squealing of brakes or the tone of a violin, are produced or conducted by waves and vibrations of solids. The field of physics, which deals with generation, propagation and radiation of oscillating motions and forces in solid bodies is called *structure-borne sound*. As compared to acoustics a much greater variety of

phenomena occurs in structure-borne sound. This is because structure-borne sound propagates in many structures and because two generic types of waves (longitudinal and transverse) and their combinations occur in solid bodies different from gases and liquids where only compression waves can be found.

2.1.7. Radiation Efficiency

One of the most important parameters for the acoustic radiation from machines is the *radiation efficiency* σ. The machine radiates into the air with a *specific impedance* $(\rho.c)_{air}$, where c is the sound velocity and ρ its density. Let the machine radiating surface be S and $\overline{\tilde{v}^2}$ be the square of the area-weighted surface normal velocity $\tilde{v}$, measured perpendicular to the radiating outer surface S, then we have

$$\sigma = \frac{P}{(\rho c)_{air} S \overline{\tilde{v}^2}}. \tag{2.20}$$

If the vibrations of the source are in-phase over domains, whose dimensions are greater than the wavelength of air, the wavelength of the radiating body is thus greater than the wavelength of air (non-compact source), then $\sigma \approx 1$. The condition of $\sigma \leq 1$ generally prevails but in certain exceptions $\sigma \geq 1$ can be experienced when the wavelength of the radiating body and the wavelength of air are almost equal.

2.1.8. Logarithmic ratios

In practice, the acoustics parameters can take very different orders of magnitude. For instance, the human ear can barely perceive by a frequency of 1000 Hz an acoustic pressure of $2 \cdot 10^{-5} Pa$ (hearing threshold level). By the same frequency with an acoustic pressure of $20 Pa$ initiates pain (pain threshold). The acoustic range between the hearing- and pain threshold extends up to 6 digits. In acoustics, logarithmic ratios are computed in order to have an easier data manipulation. According to DIN EN 21683, we have the following definitions

- *Sound Power Level*

  $$L_P(\nu) = 10 \cdot \log_{10} \frac{P(\nu)}{P_o} dB, \tag{2.21}$$

  where $P(\nu)$ is the acoustic power with a frequency ν and $P_o = 1 \cdot 10^{-12} W$ the reference power

- *Sound Pressure Level (SPL)*

  $$L_p(\nu) = 10 \cdot \log_{10} \frac{\bar{p}(\nu)^2}{p_o^2} \equiv 20 \cdot \log_{10} \frac{p(\nu)}{p_o} dB, \tag{2.22}$$

  where the field variable $p(\nu)$ is the sound pressure with a frequency ν and $p_o = 2 \cdot 10^{-5} Pa$ its reference value for air. For other mediums other than air $p_o = 1 \cdot 10^{-6} Pa$.

- *Sound Intensity Level*

$$L_I(\nu) = 10 \cdot \log_{10} \frac{I(\nu)}{I_o} dB, \tag{2.23}$$

where $I(\nu)$ is the sound intensity with a frequency ν and $I_o = 1 \cdot 10^{-12} W/m^2$ its reference value.

- *Velocity Level*

$$L_v(\nu) = 20 \cdot \log_{10} \frac{v(\nu)}{v_o} dB, \tag{2.24}$$

where the field variable $v(\nu)$ is the velocity with a frequency ν and $v_o = 1 \cdot 10^{-9} m/s$ the reference value for the velocity.

2.1.9. Acoustic directivity

The **directivity** is a measure of the radiation pattern from a source indicating how much of the total energy from the source is radiating in a particular direction.

2.1.10. Sommerfeld Condition

In acoustics, we need to handle frequently with the case in which our domain Ω is infinite. In addition to the boundary conditions on the finite boundary Γ, the solution has to fulfill regularity conditions at infinity (see Figure 2.1). This condition is derived by enclosing the object with a sphere of radius R that creates a truncated domain Ω^∞ with a boundary Γ^∞. The variation of Γ^∞ is assumed to be only dependent in the radial direction and therefore we transform our wave equation (2.13) into spherical coordinates, which yields according to *Gaul, Kögl and Wagner*

$$\phi_{,rr} + \frac{2}{r}\phi_{,r} - \frac{1}{c^2}\ddot{\phi} = 0. \tag{2.25}$$

Taking into account d'Alembert's solution in 1-D we obtain a solution as

$$\phi(r,t) = \lim_{R\to\infty} \frac{1}{R}\left[f(t - \frac{R}{c}) + g(t + \frac{R}{c})\right], \tag{2.26}$$

where f and g are two arbitrary functions with arguments that describe outgoing and incoming waves respectively. Since we are considering an infinite domain, we exclude g. Differentiating with respect to time and radius we obtain the **radiation condition** (also known as the *Sommerfeld's condition*) which consists of two parts,

1. First, we have

$$\lim_{R\to\infty}\left[R^{(\frac{D-1}{2})}(\phi_{,R} + \frac{1}{c}\dot{\phi})\right] = 0, \tag{2.27}$$

where $D = 1, 2, 3$ denotes the geometric dimension

2. Secondly, the field itself must fulfil a decay condition

$$\lim_{R\to\infty} \phi = 0, \tag{2.28}$$

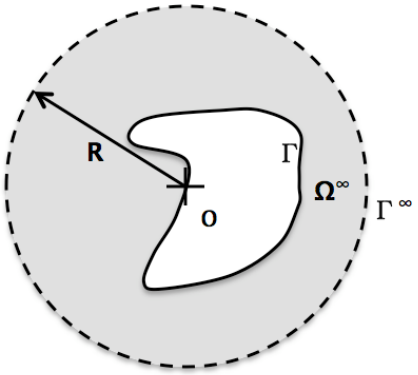

Figure 2.1.: Regularity condition at infinity (Gaul Kögl Wagner 2003)

2.1.11. Near Field / Far Field

In acoustics the **far field** is the minimum distance from where a sound source can be seen as a source that is producing a plane wave with the sound pressure and sound velocity in phase. In the **near field** this is not true and the directivity depends on the distance as well. Other definitions of far field may use the directivity as a definition, namely as the minimum distance where the directivity is independent of the distance. The distance boundary between the far field (Fraunhofer zone) and near field (Fresnel zone) is frequency-dependent.

2.2. Zero-order spherical radiator

The **zeroth-order spherical radiator** exhibits in the ideal case a tiny, compact form with relatively thick walls. The volume from this sound source changes pulsatively like a combustion engine: In the ideal case, the zeroth-order spherical radiator is the simplest basic radiator. Its surface pulses in phase outwards and inwards with the structure-borne sound velocity Vs as it can be seen in Figure 2.2. The center point of the volume M keeps its position. The radiator emits into the surrounding medium, for instance air, spherical waves due to the ideal symmetry without any directional characteristics with the excess pressure p and the velocity v according to the following Equations starting from (2.6) and (2.12)

$$\underline{p} = \rho \frac{\partial \underline{\phi}}{\partial t} = -j\hat{\phi}' \frac{w\rho}{r} \cdot e^{-jkr} \cdot e^{jwt}\,, \tag{2.29}$$

$$\underline{v} = \frac{\partial \underline{\phi}}{\partial r} = \frac{\hat{\phi}'}{r^2}(1 + jkr) \cdot e^{-jkr} \cdot e^{jwt} \,, \tag{2.30}$$

where $\underline{\phi}$ can be written in a complex form as

$$\underline{\phi} = -\frac{\hat{\phi}'}{r} \cdot e^{-jkr} \cdot e^{jwt} \,. \tag{2.31}$$

By replacing $r = d_o/2$ in (2.30), we obtain the amplitude of the potential $\hat{\phi}'$:

$$\hat{\phi}' = \hat{V_s}\frac{d_0^2}{4}\frac{1}{1 + j\frac{\pi d_0}{\lambda}} \cdot e^{+j\frac{kd_o}{2}} \,, \tag{2.32}$$

where, $k = \frac{2\pi}{\lambda}$ is the wavenumber of the emitted sound with a wavelength λ and a velocity amplitude on the sphere surface of $\hat{V_s}$.

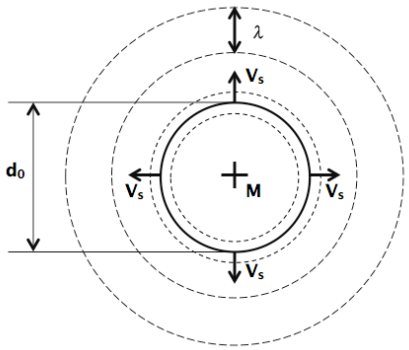

Figure 2.2.: Zeroth-order Monopole

Inserting (2.32) and $w = 2\pi c/\lambda$ into (2.29) and (2.30) , we obtain

$$\underline{p}(r,t) = -j\hat{V_s}\frac{\frac{d_0}{2}}{r}\frac{\frac{\pi d_o}{\lambda}}{1 + j\frac{\pi d_0}{\lambda}}(\rho c) \cdot e^{-jk\left(r - \frac{d_0}{2}\right)} \cdot e^{jwt} \,, \tag{2.33}$$

$$\underline{v}(r,t) = \hat{V_s}\frac{\frac{d_0}{2}}{r}\frac{1}{1 + j\frac{\pi d_0}{\lambda}}\left(\frac{\frac{d_0}{2}}{r} + j\frac{\pi d_0}{\lambda}\right) \cdot e^{-jk\left(r - \frac{d_0}{2}\right)} \cdot e^{jwt} \,. \tag{2.34}$$

By replacing $r = d_0/2$ in (2.33) and (2.34), we obtain the acoustic pressure and velocity respectively. Then substituting these equations in (2.17), yields the impedance in the surface,

$$\underline{Z}_S = \frac{\underline{p}_S}{\underline{v}_S} = j(\rho c)\frac{\frac{\pi d_0}{\lambda}}{1 + j\frac{\pi d_0}{\lambda}}. \tag{2.35}$$

The sound power P_L yields

$$P_L = A_S \cdot I_S = A_S \cdot \frac{1}{T}\int_0^T Re\{\underline{p}\}Re\{\underline{v}\}dt = A_S \cdot \underbrace{\frac{1}{2}Re\{\underline{p}\cdot\underline{v*}\}}_{I_S}, \tag{2.36}$$

$A_S \rightarrow$ the sphere surface,
$I_S \rightarrow$ the intensity radiated in the sphere surface,
$\underline{v*} \rightarrow$ the complex conjugated vector of the velocity $\underline{v}$;

According to equation $P = \frac{1}{2}|\hat{F}|^2 \cdot Re\{\frac{1}{\overline{Z}}\}$, the sound power can be written as

$$P_L = \frac{1}{2}A_S \cdot |\hat{p}_S|^2 \cdot Re\{\frac{1}{Z}\}. \tag{2.37}$$

Replacing $|\hat{p}_S|^2 = \hat{v}_S^2(\rho c)^2 \frac{\left(\frac{\pi d_0}{\lambda}\right)^2}{1+\left(\frac{\pi d_0}{\lambda}\right)^2}$; $Re\{\frac{1}{\underline{Z}_S}\} = \frac{1}{\rho c}$ and $\tilde{v}_S^2 = \frac{1}{2}\hat{v}_S^2$ into (2.37) we have

$$P_L = \underbrace{\pi d_0^2 \tilde{v}_S^2(\rho c)}_{P_K} \frac{\left(\frac{\pi d_0}{\lambda}\right)^2}{1+\left(\frac{\pi d_0}{\lambda}\right)^2}, \tag{2.38}$$

where P_K is the *structure-borne sound power*. Finally, the *radiation efficiency level* for the monopole yields

$$\sigma' = 10\log_{10}(\sigma) = 10\log_{10}\left[\frac{\left(\frac{\pi d_0}{\lambda}\right)^2}{1+\left(\frac{\pi d_0}{\lambda}\right)^2}\right] = 10\log_{10}\left[\frac{(d_0 f)^2}{\left(\frac{c}{\pi}\right)^2+(d_0 f)^2}\right]. \tag{2.39}$$

For more information, the reader should refer to [6].

2.2.1. Physical Boundary Conditions

In order to obtain a well-posed problem, we have to prescribe initial and boundary values on the surface of the radiator and at infinity . We consider the domain B with boundary S, which is divided into:

- **Dirichlet boundary**(S_{fp}) where the value of acoustic pressure p is prescribed.

$$p = \bar{p}, \qquad \delta p = 0. \tag{2.40}$$

- **Neumann boundary**, where the gradient $\frac{\partial p}{\partial \vec{n}}$ is prescribed.

$$\frac{\partial p}{\partial \vec{n}} = \vec{\nabla} p \cdot \vec{n} = -(\rho_f \dot{\vec{v}}) \cdot \vec{n}. \tag{2.41}$$

- **Robin boundary**, where a linear relation between the potential and the flux is prescribed.

$$\frac{\partial p}{\partial \vec{n}} + jw\rho G p = R(p), \tag{2.42}$$

where $R(p)$ is a linear boundary operator and $G = 1/Z$ For $G \to 0$, we obtain the Neumann problem, for $G \to \infty$ the Dirichlet problem is obtained. If Z is non-zero but finite quantity, the general impedance problem results, which describes locally reacting absorbing surfaces.

- The **Fluid-Structure Interface** (S_{fs}) where the motion of the acoustic medium is directly coupled to the motion of a solid. On such an acoustic-structural normal to the boundary the acoustic and structural media have the same displacement normal to the boundary, but the tangential motions are uncoupled. The directions of normals can be seen in Figure 2.3

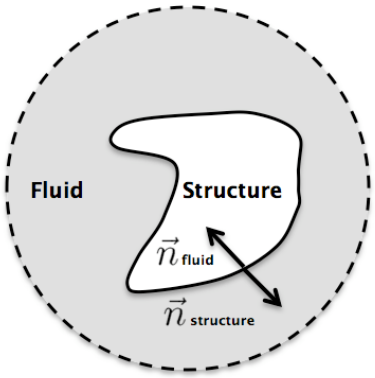

Figure 2.3.: Definition of normals in the fluid-structure interface

$$\begin{aligned}
\vec{n} \cdot \vec{u}_{Fluid} &= \vec{n} \cdot \vec{u}_{Structure}, \\
\vec{n} \cdot \dot{\vec{u}}_{Fluid} &= \vec{n} \cdot \dot{\vec{u}}_{Structure}, \\
\vec{n} \cdot \ddot{\vec{u}}_{Fluid} &= \vec{n} \cdot \ddot{\vec{u}}_{Structure}, \\
n_{interface} := n := n_{Structure} &:= -n_{Fluid}, \\
\vec{n} \cdot (\rho_f \ddot{\vec{u}})_{Fluid} &= \vec{n} \cdot (\rho_f \ddot{\vec{u}})_{Structure}.
\end{aligned} \tag{2.43}$$

These formulas assure that two conditions are fulfilled in the interface. The continuity of particle velocities and the equilibrium of reaction forces.

- The **Radiating acoustic boundary** (S_{fi}) Often acoustic media extend sufficiently far from the region of interest that they can be modeled as infinite in extent. In such cases it is convenient to truncate the computational region and apply a boundary condition to simulate waves passing exclusively outward from the computational region.

$$\vec{n} \cdot (\rho_f \ddot{\vec{v}})_{Fluid} = \frac{\rho_f}{c_1}\dot{p} + \frac{\rho_f}{a_1}p, \tag{2.44}$$

where $\frac{1}{a_1}$ and $\frac{1}{c_1}$ are admittance parameters which are defined by

$$\frac{1}{c_1} = \left[\frac{f}{\sqrt{\rho_f K_f}}\right]; \frac{1}{a_1} = f\left[\frac{\beta}{\rho_f} + \frac{\gamma}{2\rho_f\sqrt{\rho_f K_f}}\right]. \tag{2.45}$$

The values of the parameters f and β vary with the geometry of the boundary of the radiating surface of the acoustic medium.

2.3. FEM Formulation

The equilibrium equation for small motions of a compressible, adiabatic fluid with velocity-dependent momentum losses is taken to be

$$\frac{\partial p}{\partial \mathbf{x}} + \gamma(\mathbf{x}, \theta_i)\dot{\mathbf{u}}^f + \rho_f(\mathbf{x}, \theta_i)\ddot{\mathbf{u}}^f = 0. \tag{2.46}$$

This is the general definition in ABAQUS [1], where

p	$\rightarrow$	the excess pressure in the fluid;
$\mathbf{x}$	$\rightarrow$	the spatial position of the fluid particle;
$\dot{\mathbf{u}}^f$	$\rightarrow$	the fluid particle velocity;
$\ddot{\mathbf{u}}^f$	$\rightarrow$	the fluid particle acceleration;
ρ_f	$\rightarrow$	the density of the fluid;
γ	$\rightarrow$	the "volumetric drag" (force per unit volume per velocity); and
θ_i	$\rightarrow$	i independent field variables such as temperature, humidity of air, or salinity of water on which ρ_f and γ may depend.

2.3.1. Variational statement

An equivalent weak form for the equation of motion neglecting effects of *volumetric drag* γ, is derived by

$$\frac{1}{K_f}\ddot{p} - \frac{\partial}{\partial x}\cdot\left(\frac{1}{\rho_f}\frac{\partial p}{\partial x}\right) = 0, \qquad K_f = \rho_f \cdot c^2 \rightarrow \text{bulk modulus} \tag{2.47}$$

which is derived from (2.2) and from the constitutive equation of an inviscid, linear and compressible fluid, which is given by

$$p = -K_f(x,\theta_i)\frac{\partial}{\partial x}\cdot u^f. \tag{2.48}$$

Introducing an arbitrary variational field, δp, as a weighting function and integrating over the fluid in a 3D-model yields

$$\int\limits_{V_{Fluid}} \delta p\left[\frac{\ddot{p}}{c^2} - \Delta p\right] dV = 0 \qquad \rightarrow \qquad \text{Weak form} \tag{2.49}$$

Green's 1^{st} identity allows this to be rewritten as

$$\int\limits_{V_{Fluid}} \left[\frac{1}{c^2}\ddot{p}\delta p + \vec{\nabla}\delta p\cdot\vec{\nabla}p\right] dV - \int\limits_{\Gamma_{Fluid}} \delta p(\vec{n}_{Fluid}\cdot\vec{\nabla}p)d\Gamma = 0. \tag{2.50}$$

Now substituting the Neumann boundary condition, we obtain

$$\int\limits_{V_{Fluid}} \left[\frac{1}{c^2}\ddot{p}\delta p + \vec{\nabla}\delta p\cdot\vec{\nabla}p\right] dV + \int\limits_{\Gamma_{Fluid-Neumann}} \delta p(\rho_f\dot{\vec{v}})\vec{n}_{Fluid}d\Gamma = 0\ . \tag{2.51}$$

These definitions of the boundary term, $\vec{n}\cdot(\rho\dot{\vec{u}})_{Fluid}$, are introduced into (2.51) to give the final variational statement for the acoustic medium (this is equivalent to the virtual work statement for the structure):

$$\int\limits_{V_{Fluid}} \left[\delta p\left(\frac{1}{c^2}\ddot{p}\right) + \vec{\nabla}\delta p\cdot\vec{\nabla}p\right] dV + \int\limits_{S_{fi}} \delta p\left(\frac{\rho}{c_1}\dot{p} + \frac{\rho}{a_1}p\right) dS + \\ + \int\limits_{S_{fs}} \delta p\cdot\vec{n}_{Fluid}\cdot(\rho_f\ddot{\vec{u}})_{Str}dS = 0. \tag{2.52}$$

The structural behavior is defined by the virtual work equation,

$$\int\limits_V \bar{\bar{\sigma}} : \delta\bar{\bar{\varepsilon}}dV + \int\limits_V \rho_s\ddot{\vec{u}}_{Str}\cdot\delta\vec{u}_{Str}dV - \int\limits_{\Gamma_t} \vec{t}\cdot\delta\vec{u}_{Str}dA + \int\limits_{\Gamma_{fs}} \underbrace{p\vec{n}\cdot\delta\vec{u}_{Str}dA}_{\text{Coupling}} = 0, \tag{2.53}$$

where

σ	$\rightarrow$	the stress at a point in the structure,
p	$\rightarrow$	the pressure acting on the fluid-structural interface,
$\vec{n}$	$\rightarrow$	the outward normal to the structure,
ρ_s	$\rightarrow$	the density of the structure,
$\ddot{\vec{u}}_{Str}$	$\rightarrow$	the acceleration of a point in the structure,
$\vec{t}$	$\rightarrow$	the surface traction applied to the structure,
δu_{Str}	$\rightarrow$	variational displacement field, and
$\delta\varepsilon$	$\rightarrow$	the strain variation that is compatible with δu_{Str}.

For simplicity in this equation all other loading terms except the fluid pressure and surface traction $\vec{t}$ have been neglected: they are imposed in the usual way.

2.3.2. Discretized Finite Element Method

Generally, an important ingredient of the fully coupled analysis is that fluid domain can be meshed with another discretization than the one from the structure. Completely different meshes are thus usually employed for the fluid and the structure, and they must be able to transmit only normal traction. The tangential traction is set to zero. Although the meshes may be nodally nonconforming at the tied surfaces, mesh refinement affects the accuracy of the coupled solution. In acoustic-solid problems the mesh refinement depends on the wave speeds in the two media. The mesh for the medium with the lower wave speed should generally be more refined and, therefore, should be the slave surface

The equations (2.52) and (2.53) define the variational problem for the coupled fields u_{str} and p. The problem is discretized by introducing interpolation functions: in the fluid $p = H^P p^P,\ P = 1, 2...$ up to the number of pressure nodes and in the structure $u_{str} = N^N u^N,\ N = 1, 2...$ up to the number of displacement degrees of freedom. In these and the following equations we assume summation over the superscripts that refer to the degrees of freedom of the discretized model. We also use the superscripts P, Q to refer to pressure degrees of freedom in the fluid and N, M to refer to displacement degrees of freedom in the structure.

We use Galerkin method for the structural system; the variational field has the same form as the displacement: $\delta u_{str} = N^N \delta u^N$. For the fluid we use $\delta p = H^P \delta p^P$ but with the subsequent Petrov-Galerkin substitution

$$\delta p^P = \frac{d^2}{dt^2}(\delta \hat{p}^P).$$

The new function $\delta \hat{p}^P$, as explained in Abaqus Theory Manual [1], makes the single variational equation obtained from summing (2.52) and (2.53) dimensionally consistent:

$$\begin{aligned} -\delta \hat{p}^P \{(M_f^{PQ})\ddot{p}^Q + (C_f^{PQ} + C_{fi}^{PQ})\dot{p}^Q + (K_f^{PQ} + K_{fi}^{PQ})p^Q + S_{fs}^{PM}\ddot{u}^M\} \\ +\delta u^N \{I^N + M^{NM}\ddot{u}^M + \left[S_{fs}^{QN}\right]^T p^Q - P^N\} = 0. \end{aligned} \tag{2.54}$$

where, for simplicity, we have introduced the following definitions:

$$
\begin{aligned}
M_f^{PQ} &= \int_{V_f} \tfrac{1}{c^2} H^P H^Q dV, & C_f^{PQ} &= \int_{V_f} \tfrac{\gamma}{\rho_f}\tfrac{1}{c^2} H^P H^Q dV,\\
C_{fi}^{PQ} &= \int_{S_{fi}} \tfrac{\rho_f}{c_1} H^P H^Q dS, & K_f^{PQ} &= \int_{V_f} \tfrac{\partial H^P}{\partial x}\cdot\tfrac{\partial H^Q}{\partial x} dV,\\
K_{fi}^{PQ} &= \int_{S_{frs}} \tfrac{\rho_f}{a_1} H^P H^Q dS, & S_{fs}^{PM} &= \int_{S_{fs}} \rho_f H^P \vec{n}_{Fluid}\cdot N^M dS,\\
M^{NM} &= \int_V \rho_s N^N \cdot N^M dV, & I^N &= \int_V \beta^N : \sigma dV,\\
S_{fs}^{QN} &= \int_{S_{fs}} H^Q \vec{n}_{Structure}\cdot N^N dS, & P^N &= \int_{S_t} N^N \cdot t dS,
\end{aligned}
$$

The strain interpolator is β^N. This equation defines the discretized model. We see that the volumetric drag-related terms are "mass-like"; i.e., proportional to the fluid element mass matrix.

In the case of coupled systems where the forces on the structure due to the fluid $\left[S_{fs}^{QN}\right]^T p^Q$ are very small compared to the rest of the structural forces, the system can be solved in a "sequentially coupled" manner. The structural equations can be solved with the $\left[S_{fs}^{QN}\right]^T p^Q$ term omitted; i.e., in an analysis without fluid coupling. Subsequentially, the fluid equations can be solved, with $\left[S_{fs}^{PM}\right] \ddot{u}^M$ imposed as a boundary condition. This two-step analysis is less expensive and advantageous for systems such as stiff metal structures surrounded by air.

2.3.3. Time integration

The equations are integrated through time using the standard implicit and explicit integration dynamic integration options in ABAQUS. From the implicit integration operator we obtain relations between the variations of the solution variables (here represented by f) and their time derivatives:

$$D_a \overset{Def}{=} \frac{\delta \ddot{f}}{\delta f} = \frac{\delta p^p}{\delta \hat{p}^p}, \tag{2.55}$$

$$D_v \overset{Def}{=} \frac{\delta \dot{f}}{\delta f}, \tag{2.56}$$

The equation of evolution of the degrees of freedom can be written for the implicit case as

$$
\begin{aligned}
-\delta\hat{p}^P \frac{1}{D_a}\{(M_f^{PQ})\ddot{p}^Q + (C_f^{PQ} + C_{fi}^{PQ})\dot{p}^Q + (K_f^{PQ} + K_{fi}^{PQ})p^Q + S_{fs}^{PM}\ddot{u}^M\}&\\
+\delta u^N\{I^N + M^{NM}\ddot{u}^M + \left[S_{fs}^{QN}\right]^T p^Q - P^N\} = 0,&
\end{aligned}
$$

The linearization of this equation yields

$$
\begin{aligned}
-\delta\hat{p}^P\{(M_f^{PQ}) + \frac{D_v}{D_a}(C_f^{PQ} + C_{fi}^{PQ}) + \frac{1}{D_a}(K_f^{PQ} + K_{fi}^{PQ})\}dp^Q + \delta p^P S_{fs}^{PM} du^M&\\
+\delta u^N \left[S_{fs}^{QN}\right]^T dp^Q + \delta u^N\{K^{NM} + D_a M^{NM}\}du^M = 0,&
\end{aligned}
$$

where dp and du are the corrections to the solution obtained from the Newton iteration, K^{NM} is the structural stiffness matrix.

Applications of acoustic-fluid/structure interactions are found whenever the fluid can be modeled to be inviscid and to undergo only relatively small particle motions. Some examples are the analysis of pressure waves in a piping system, a fluid sloshing in a tank, and sound waves traveling through fluid-solid media. Since the matrices are symmetrical, fine finite-element meshes can be used, allowing detailed effects to be simulated.

2.3.4. Eigenvalue extraction and Modal analysis

There are many areas of structural analysis in which it is essential to be able to extract the eigenvalues of the system and, hence, obtain its natural frequencies of vibration or investigate possible bifurcations that may be associated with kinematic instabilities. Once the modes are available, their orthogonality property allows the linear response of the structure to be constructed as the response of a number of single degree of freedom systems. This opens the way to several response evaluation methods that are computationally inexpensive and provide useful insight into the dynamic behavior of the structure.

The mathematical eigenvalue problem is a classical field of study, and much work has been devoted to providing eigenvalue extraction methods. The eigenvalue problems arising out of finite element models are a particular case: they involve large but usually narrowly banded matrices, and only a small number of eigenpairs are usually required. For many important cases the matrices are symmetric.

In general, for a damped system, excited by a force, we have

$$\underline{\underline{M}}\,\underline{\ddot{U}} + \underline{\underline{C}}\,\underline{\dot{U}} + \underline{\underline{K}}\,\underline{U} = \underline{F}, \qquad \rightarrow \qquad \text{Equation of motion} \tag{2.57}$$

where

$\underline{\underline{M}}$ $\rightarrow$ the global mass matrix,
$\underline{\underline{C}}$ $\rightarrow$ the global damping matrix,
$\underline{\underline{K}}$ $\rightarrow$ the global stiffness matrix, and,
$\underline{F}$ $\rightarrow$ the global force vector,

In the study of machine acoustics, periodic procedures are of interest and hence according to Fourier's theorem, we may assume a pure harmonic excitation. With this assumption, the force vector $\underline{F}$ can be expressed as

$$\underline{F} = \underline{\hat{F}} exp(i\Omega t), \tag{2.58}$$

where F is a vector of the active force amplitudes in the element-nodes of the structure and Ω is the angular frequency of excitation.

In general, the vector $\hat{F}$ is assumed to be complex, since in this way, different, arbitrary phases of the concentrated loads in the Element nodes are permitted. The

expression for the required vector of nodal deflections is given by

$$\underline{U} = \underline{\hat{U}} exp(i\Omega t). \tag{2.59}$$

Substituting (2.58) and (2.59) in (2.57) yields

$$-\Omega^2 \underline{\underline{M}}\,\underline{\hat{U}} + i\Omega \underline{\underline{C}}\,\underline{\hat{U}} + \underline{\underline{K}}\,\underline{\hat{U}} = \underline{\hat{F}}. \tag{2.60}$$

A direct solution of the complex system of equations is computationally very expensive. Hence, for the determination of stationary, forced vibrations, we often adopt the method of mathematical Modal Analysis. Generally, Modal Analysis is defined as a method, which by means of a mathematical or experimental way, enables the determination of an approximation of the Eigenfunctions of a continuous oscillator. These approximations are known as the Eigenforms or the Modes. Now, by means of the mathematical Modal Analysis, we shall solve the general Eigenvalue problem for an undamped system with $\underline{F} = 0$,

$$(\underline{\underline{K}} - w_i^2 \underline{\underline{M}})\underline{\Phi}_i = 0, \qquad 1 \leq i \leq n_{\text{mod}}, \tag{2.61}$$

where n_{mod}, $\rightarrow$ the number of eigenvalues of the undamped system,
w_i $\rightarrow$ the eigenvalues, and,
$\underline{\Phi}_i$ $\rightarrow$ the eigenvectors of the corresponding modes,

Since the stiffness- and mass matrices are positive-semi-definite and positive-definite respectively, it shows that the eigenvalues, w_i^2, are positive. The values of w_i are hence real.

The number of modes determined, n_{mod} and the corresponding eigenvalues are in general much smaller than the number of global degrees of freedom, $N_f (n_{\text{mod}} << N_f)$, since the complete calculation of all N_f modes and the corresponding eigenvalues is numerically very expensive.

After the determination of the modes $\underline{\Phi}_i$ and the corresponding Eigenvalues w_i^2 of the general eigenvalue problem, we can now proceed to the method of mathematical Modal analysis. For this, all the n_{mod} determined modes $\underline{\Phi}_i$ are combined in a (N_f, n_{mod}) matrix.

$$\underline{\underline{\Phi}} = \left[\underline{\Phi}_1 \quad \underline{\Phi}_2 \ldots \quad \underline{\Phi}_i \ldots \quad \underline{\Phi}_{n_{\text{mode}}}\right], \tag{2.62}$$

Thereafter, the modal degrees of freedom or the general modal co-ordinates are introduced by the following modal transfomation,

$$\underline{\underline{\Phi}}\,\underline{\hat{X}} := \underline{\hat{U}}, \tag{2.63}$$

Since $\underline{\underline{\Phi}}$ is a (N_f, n_{mod})-matrix, the above transformation builds a n_{mod}-rows vector $\underline{\hat{X}}$. The number of components in the vector $\underline{\hat{X}}$ is equal to the number of modes or eigenvalues that are determined by the general eigenvalue problem. Furthermore, the Eigenvalues are arranged in the form of a diagonal matrix,

$$\underline{\underline{w}}^2 := diag\left[w_i^2\right], \quad i = 1, 2, 3 \ldots n_{\text{mod}}, \tag{2.64}$$

Correspondingly, $\underline{\underline{\Omega}}^2$ is also a diagonal matrix, whose diagonal is occupied n_{mod} times with the square of the angular excitation frequency Ω^2. Next, the product of all the damping coefficients and the corresponding angular eigenfrequencies are arranged in a n_{mod}-diagonal matrix

$$\underline{\underline{\xi}}\,\underline{\underline{w}} := diag\,[\xi_i w_i] \tag{2.65}$$

Inserting (2.63) in (2.60) and multiplying with the matrix $\underline{\underline{\Phi}}^T$, we obtain the equation in the following form,

$$\left(-\Omega^2 \underline{\underline{\Phi}}^T \underline{\underline{M}}\,\underline{\underline{\Phi}} + i\Omega \underline{\underline{\Phi}}^T \underline{\underline{C}}\,\underline{\underline{\Phi}} + \underline{\underline{\Phi}}^T \underline{\underline{K}}\,\underline{\underline{\Phi}}\right) \underline{\hat{X}} = \underline{\hat{R}}, \tag{2.66}$$

where

$$\begin{array}{rcl} \underline{\underline{\Phi}}^T \underline{\underline{M}}\,\underline{\underline{\phi}} & \rightarrow & (n_{\text{mod}}, n_{\text{mod}})\text{diagonalized nodal mass matrix,} \\ \underline{\underline{\Phi}}^T \underline{\underline{C}}\,\underline{\underline{\Phi}} & \rightarrow & (n_{\text{mod}}, n_{\text{mod}})\text{diagonalized nodal damping matrix,} \\ \underline{\underline{\Phi}}^T \underline{\underline{K}}\,\underline{\underline{\Phi}} & \rightarrow & (n_{\text{mod}}, n_{\text{mod}})\text{diagonalized nodal stiffness matrix, and} \\ \underline{\hat{R}} & \rightarrow & \text{the vector of the nodal force.} \end{array}$$

Finally, the modified-force vector is introduced,

$$\underline{\hat{R}} = \underline{\underline{\Phi}}^T\, \underline{\hat{F}}, \tag{2.67}$$

which reduces the N_f components of the force-amplitude-vector $\underline{\hat{f}}$ to n_{mod} general forces, which are summarized in the vector $\underline{\hat{R}}$.

Thus, from the known vector $\underline{\hat{R}}$ of nodal forces, and the matrix $\underline{\underline{\Phi}}$ of the modes, we can calculate the vector $\underline{\hat{X}}$ of nodal displacements.

2.3.5. Submodeling

Submodeling is the technique of studying a local part of a model with a refined mesh, based on interpolation of the solution from an initial, global model onto appropriate parts of the boundary of the submodel. The **global model** is the model whose solution is interpolated onto the relevant parts of the boundary of the **submodel**. The *Driven variables* are defined as those variables in the submodel that are constrained to match results from the global model. This method is most useful when it is necessary to obtain an accurate, detailed solution in the local region and the detailed modeling of that local region has negligible effect on the overall solution Two forms of the submodeling technique are available in Abaqus.

- *Node-based submodeling*: transfers node-located solution variables, most commonly displacements, from global model nodes to submodel nodes.
- *Surface-based submodeling*: uses the stress field to interpolate global model results onto the submodel integration points.

  In Abaqus the node-based submodeling technique can be used to analyze an acoustic model driven by displacements from a structural, global model when the acoustic fluid has negligible effect on the structural solution.

2.3.6. TIE - Fluid-Structure Interaction

A surfaced-based **tie constraint** in ABAQUS [1] ties two surfaces together for the duration of the simulation. This constraint can be used to make translational and rotational motions as well as all other active degrees of freedom equal for a pair of surfaces. One surface in the constraint is designated to be the slave surface; the other surface is the master surface. By default, nodes are tied only where the surfaces are close to one another. In the case of structural-acoustic constraints appropriate relations between the acoustic pressure on the fluid surface and displacements on the solid surface are formed internally. The displacements and/or pressure degrees of freedom on the surfaces are the only ones affected; rotations are ignored by the tie constraint in this case. The way of handling the degrees of freedom is different depending on which surface is the master and which one is the slave.

- If the **fluid medium surface** is designated as the *slave*, we constrain values at each fluid node to be an average of the values at nearby master surface nodes. The condition is enforced at the slave nodes, resulting in displacement degrees of freedom added to the fluid slave surface. These slave displacements are constrained by the master displacements and thereby eliminated. The slave pressures are not constrained directly.
- On the other hand, if the **solid medium surface** is designated as the *slave*, the values on this surface are constrained to equal the values interpolated from the master surface. The fluid-solid coupling condition is again enforced at the slave nodes, resulting in acoustic pressure degrees of freedom added to the solid slave surface. These slave pressures are constrained by the master surface acoustic pressures and eliminated. The slave displacements are not constrained directly.

This behavior is summarized in Table (2.1)

Table 2.1.: Possible Slave-Master surfaces pairings

Slave Surface	Master Surface	Degrees of freedom tied
Acoustic	Stress	Translations
Stress	Acoustic	Acoustic Pressure

2.4. BEM Formulation

The boundary element method in acoustics is a numerical technique for calculating the sound radiated by a vibrating body or for predicting the sound field inside of a cavity such as a vehicle interior. The BEM is becoming a popular numerical technique for acoustical modeling in industry. The major advantage of this method is that only the boundary surface (e.g., the exterior of the vibrating body) needs to be modeled with a mesh of elements. Besides, for infinite-domain problems, such as radiation from a vibrating structure, the so-called Sommerfeld radiation condition is automatically

fulfilled. In other words, there is no need to create a mesh to approximate this radiation condition as in FEM. A typical BEM input file consists of a surface, the fluid density, speed of sound, and frequency. The output of the BEM includes the sound pressure distribution on the surface of the body and at other points in the field, the sound intensity, and the sound power.

The BEM is a relatively new tool compared to other acoustic analysis techniques such as the FEM. Much progress has been made in enhancing and tailoring the BEM for acoustics. Similar to the FEM, however, it is computationally and memory intensive, perhaps more so for certain applications.

2.4.1. Direct and Indirect BEM

The *Direct BEM* is ruled by the Direct Boundary Integral Formulation. The DBEM relates the pressure at any point of an acoustic field to the pressure and normal velocity distribution on the closed boundary surface of the acoustic domain. The term "direct" indicates that the boundary variables already mentioned have a direct physical meaning. When using this method, a distinction between an interior and exterior problem has to be made.

On the other hand, the *Indirect BEM* is ruled by the Indirect Boundary Integral Formulation. The IBEM works with sources from which the direct variables have to be concluded

$$\underbrace{\int \Phi(x,\xi)q(x)d\Gamma}_{\text{Single layer potential}} \qquad \underbrace{\int \frac{\partial \Phi}{\partial n}p(x)d\Gamma}_{\text{Double layer potential}} \quad . \tag{2.68}$$

The term "indirect" indicates that these boundary variables have an indirect physical meaning. The *single layer potential* function can be regarded as a distribution of monopole sources on the boundary surface while the *double layer potential* function as one of dipole sources.

The indirect approach is the one used in this study since in the transient acoustics in Virtual.Lab it is the only option available.

2.4.2. Hybrid Displacement Boundary Element Method

The *Hybrid Displacement Boundary Element Method* (HDBEM) for the time domain leads to symmetric systems of equations with time-invariant mass and stiffness matrices [5]. The HDBEM formulation for the fluid domain is derived from Hamilton's Principle, which is derived at the same time from the principle of Lagrange-d'Alembert, stating that the solution of a boundary value problem is characterized by stationarity of the time integral over the Lagrangian function given for a compressible fluid in the domain Ω with boundary Γ. The generalized functional used in the HDBEM consists of terms for the kinetic and potential energy, a work term leading to the Neumann boundary condition, and the continuity term of the domain

and boundary variables:

$$\mathcal{H}^{\mathrm{HD}}(\phi,\tilde{\phi},\lambda)=\int_{t_0}^{t_1}\left[\frac{1}{2}\int_{\Omega}\rho_0(\phi_{,i}\phi_{,i}-\frac{1}{c^2}\dot{\phi}\dot{\phi})d\Omega-\int_{\Gamma_\psi}\rho_0\bar{\psi}\tilde{\phi}d\Gamma+\int_{\Gamma}\lambda(\tilde{\phi}-\phi)d\Gamma\right]dt, \tag{2.69}$$

with the subsidiary Dirichlet condition

$$\tilde{\phi}=\bar{\phi}\qquad on\qquad \Gamma_\phi, \tag{2.70}$$

where,

ϕ $\rightarrow$ the velocity potential in the domain,
$\tilde{\phi}$ $\rightarrow$ the velocity potential in the boundary,
$\bar{\phi}$ $\rightarrow$ the dirichlet boundary condition for the velocity potential,
λ $\rightarrow$ the Lagrange multiplier,
$\bar{\psi}$ $\rightarrow$ the Neumann boundary condition for the flux, and
ρ_0 $\rightarrow$ the equilibrium density

Performing the first variation of the kinetic energy term and applying the Gauß' theorem, yields:

$$\begin{aligned}\frac{1}{2}\delta\int_{t_0}^{t_1}\int_{\Omega}\rho_0\phi_{,i}\phi_{,i}d\Omega dt &= \int_{t_0}^{t_1}\int_{\Omega}\rho_0\phi_{,i}\delta(\phi_{,i})d\Omega dt\\ &= \int_{t_0}^{t_1}\left[\int_{\Gamma}\rho_0\phi_{,i}n_i\delta\phi d\Gamma-\int_{\Omega}\rho_0\phi_{,ii}\delta\phi d\Omega\right]dt,\end{aligned} \tag{2.71}$$

Now, applying the first variation for the potential energy term and taking into account that the variation at the time boundaries vanishes, $\delta\phi(t_p)=\delta\phi(t_1)=0$, we have:

$$\frac{1}{2}\delta\int_{t_o}^{t_1}\int_{\Omega}\frac{\rho_0}{c^2}\dot{\phi}\dot{\phi}d\Omega dt=\int_{t_o}^{t_1}\int_{\Omega}\frac{\rho_0}{c^2}\dot{\phi}\delta\dot{\phi}d\Omega dt=-\int_{t_o}^{t_1}\int_{\Omega}\frac{\rho_0}{c^2}\ddot{\phi}\delta\phi d\Omega dt, \tag{2.72}$$

Provided that the variation on the adjoint boundaries vanish, $\delta\phi=0$ on Γ_ϕ and $\delta\psi=0$ on Γ_ψ, the first variation of the whole functional reads

$$\begin{aligned}\delta\mathcal{H}^{\mathrm{HD}} &= \int_{t_0}^{t_1}\Big[-\int_{\Omega}\rho_0(\phi_{,ii}-\frac{1}{c^2}\ddot{\phi})\delta\phi d\Omega+\int_{\Gamma}(\rho_0\psi-\lambda)\delta\phi d\Gamma+\\ &\quad\int_{\Gamma_\psi}(-\rho_0\bar{\psi}+\lambda)\delta\tilde{\phi}d\Gamma+\int_{\Gamma}(\tilde{\phi}-\phi)\delta\lambda d\Gamma\Big]dt=0.\end{aligned} \tag{2.73}$$

The Lagrange multiplier can be identified as

$$\lambda \equiv \rho_0 \tilde{\psi}. \tag{2.74}$$

Then, the domain variables are approximated by:

$$\phi(x,t) = \sum_{n=1}^{N} \phi_n^*(x,\xi)\gamma_n(t), \tag{2.75}$$

$$\psi(x,t) = \sum_{n=1}^{N} \psi_n^*(x,\xi)\gamma_n(t), \tag{2.76}$$

where, $\phi_n^*(x,\xi)$ and $\psi_n^*(x,\xi)$ are spatial fundamental solutions that are weighted by the time dependent parameter $\gamma_n(t)$. The node points $\xi^{(n)}, n = 1, ..., N$ are collocated at the nodes of the boundary discretisation, since this provides an easier way to couple another domain discretised with the FEM. $\gamma_n(t)$ are unknowns, and the static fundamental solutions are singular solutions of Laplace's equation with a Dirac distribution as the right hand side:

$$\phi_{,ii}(x,\xi) = -\delta(x,\xi), \tag{2.77}$$

(2.75) and (2.76) can be written in matrix notation as:

$$\underline{\phi}(x,t) = \underline{\underline{\mathbf{\Phi}}}^{\mathbf{T}}(x,\xi)\underline{\gamma}_n(t), \tag{2.78}$$

$$\underline{\Psi}(x,t) = \underline{\underline{\mathbf{\Psi}}}^{\mathbf{T}}(x,\xi)\underline{\gamma}_n(t), \tag{2.79}$$

where $\underline{\underline{\phi}}^*$ and $\underline{\underline{\psi}}^*$ contain the static fundamental solutions and their normal derivatives. The potential $\underline{\tilde{\phi}}$ and velocity fields $\underline{\tilde{\psi}}$ on the boundary are approximated by the same shape functions in the matrix $\underline{\underline{\mathbf{\Phi}}}$ and the corresponding time-dependent nodal vectors $\underline{\check{\phi}}(t)$ and $\underline{\check{\psi}}(t)$:

$$\underline{\tilde{\phi}}(x,t) = \underline{\underline{\mathbf{\Phi}}}^T(x)\underline{\check{\phi}}(t), \tag{2.80}$$

$$\underline{\tilde{\psi}}(x,t) = \underline{\underline{\mathbf{\Phi}}}^T(x)\underline{\check{\psi}}(t). \tag{2.81}$$

Replacing (2.78) and (2.81) in (2.73), yields:

$$\begin{aligned}\delta\mathcal{H}^{\mathrm{HD}} = \int_{t_0}^{t_1} \rho_0 \Big[&-\delta\gamma^T \int_\Omega \phi^*_{,ii}\phi^{*^T} d\Omega\gamma + \delta\gamma^T \int_\Omega \frac{1}{c^2}\phi^*\phi^{*^T} d\Omega\ddot{\gamma} + \\ &+\delta\gamma^T \int_\Gamma \phi^*\psi^{*^T} d\Gamma\gamma - \delta\gamma^T \int_\Gamma \phi^*\mathbf{\Phi}^T d\Gamma\check{\psi} - \delta\check{\phi}^T \int_{\Gamma_\psi} \mathbf{\Phi}\bar{\psi} d\Gamma + \\ &+\delta\check{\psi}^T \int_{\Gamma_\psi} \mathbf{\Phi}\mathbf{\Phi}^T d\Gamma\check{\psi} + \delta\check{\psi}^T \int_\Gamma \mathbf{\Phi}\mathbf{\Phi}^T d\Gamma\check{\phi} - \delta\check{\phi}^T \int_\Gamma \mathbf{\Phi}\phi^{*^T} d\Gamma\gamma \Big] dt = 0.\end{aligned} \tag{2.82}$$

Here, Φ and Ψ have weak and strong singularities. To avoid these singularities at the load points $\xi^{(i)}$, they are excluded from the domain by spheres (3D) or circles (2D) of radius ε, see Figure 2.4. A modified domain Ω' with boundary Γ' is obtained. To retrieve the original domain, a limit process for ε is carried out

$$\lim_{\varepsilon \to 0} \Omega' = \Omega \qquad \textit{and} \qquad \lim_{\varepsilon \to 0} \Gamma' = \Gamma.$$

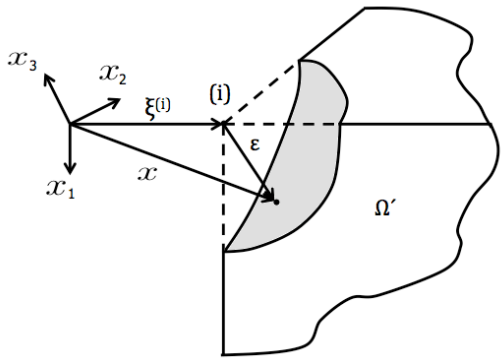

Figure 2.4.: Domain modification in the Hybrid BEM

To eliminate the first two terms (domain integrals) we use first the following domain approximation by modificating the boundary and excluding the load points $\xi^{(i)}$:

$$\lim_{\varepsilon \to 0} \int_{\Omega'} \rho_0 \underbrace{\phi^*_{n,jj}}_{\delta_n(x,\xi)} \phi^*_m d\Omega \gamma_m = 0. \tag{2.83}$$

Then we assume that we are working with a harmonic differential operator ($\phi^*_{,ii} = 0$) and define a function v^*

$$v^*_{,ii}(x,\xi) + \phi^*(x,\xi) = 0, \tag{2.84}$$

and by deriving the weak form of this function with the weighting function $\phi^*(x,\xi)$, we obtain the Green's formula

$$\begin{aligned} \int_\Omega (v^*_{,ii} + \phi^*)\phi^* d\Omega \;\; &= \;\; \int_\Gamma \left(\frac{\partial c^*}{\partial n}\phi^* - v^* \frac{\partial \phi^*}{\partial n} \right) + \\ &+ \int_\Omega (v^* \phi^*_{,ii} + \phi^* \phi^*) d\Omega. \end{aligned} \tag{2.85}$$

Finally we obtain the boundary integral formulation,

$$\delta\mathcal{H}^{\mathrm{HD}} = \int_{t_0}^{t_1} \rho_0 \Big[\delta\gamma^T \Big(\int_\Gamma \frac{1}{c^2} \Big(\mathbf{v}^* \psi^{*^T} - \frac{\partial v^*}{\partial n} \phi^{*^T} \Big) d\Gamma \ddot{\gamma} + \\ + \int_\Gamma \phi^* \psi^{*^T} d\Gamma \gamma - \int_\Gamma \phi^* \mathbf{\Phi}^T d\Gamma \check{\psi} \Big) - \\ - \delta\check{\phi}^T \Big(\int_{\Gamma_\psi} \mathbf{\Phi} \bar{\psi} d\Gamma - \delta\check{\psi}^T \int_{\Gamma_\psi} \mathbf{\Phi}\mathbf{\Phi}^T d\Gamma \check{\psi} \Big) + \\ + \delta\check{\psi}^T \Big(\int_\Gamma \mathbf{\Phi}\mathbf{\Phi}^T d\Gamma \check{\phi} - \int_\Gamma \mathbf{\Phi} \phi^{*^T} d\Gamma \gamma \Big) \Big] dt = 0, \tag{2.86}$$

where the vector $\mathbf{v}^*$ contains the function $v^*(x, \xi^{(i)})$ with $i = 1, 2, \ldots, N$. For 3-D problems, this yields

$$v^* = -\frac{r(x,\xi)}{8\pi}, \qquad \frac{\partial v^*}{\partial n} = -\frac{1}{8\pi} \frac{\partial r(x,\xi)}{\partial n}. \tag{2.87}$$

Taking the following brief notation

$$\underline{\underline{\mathbf{N}}} = \lim_{\varepsilon \to 0} \int_{\Gamma'} \frac{1}{c^2} \left(\underline{\mathbf{v}}^* \underline{\underline{\psi}}^{*^T} - \frac{\partial \underline{\mathbf{v}}^*}{\partial n} \underline{\underline{\phi}}^{*^T} \right) d\Gamma, \tag{2.88}$$

$$\underline{\underline{\mathbf{F}}} = \lim_{\varepsilon \to 0} \int_{\Gamma'} \underline{\underline{\phi}}^* \underline{\underline{\psi}}^{*^T} d\Gamma, \quad \underline{\underline{\mathbf{G}}} = \lim_{\varepsilon \to 0} \int_{\Gamma'} \underline{\underline{\phi}}^* \underline{\underline{\Phi}}^{*^T} d\Gamma, \tag{2.89}$$

$$\underline{\underline{\mathbf{L}}} = \lim_{\varepsilon \to 0} \int_{\Gamma} \underline{\underline{\Phi}}\, \underline{\underline{\Phi}}^T d\Gamma, \qquad \underline{\boldsymbol{f}} = \int_{\Gamma_\psi} \underline{\underline{\Phi}}\, \underline{\bar{\psi}} d\Gamma, \tag{2.90}$$

by introducing the equations (2.88), (2.89) and (2.90) in (2.86), the principle is expressed as

$$\delta\mathcal{H}^{\mathrm{HD}}(\phi, \tilde{\phi}, \tilde{\psi}) = \int_{t_0}^{t_1} \rho_0 \quad \Big[\quad \delta\gamma^T (\mathbf{N}\ddot{\gamma} + \mathbf{F}\gamma - \mathbf{G}\check{\psi}) + \\ + \quad \delta\check{\psi}^T (\mathbf{L}^T \check{\psi} - \boldsymbol{f}) + \\ + \quad \delta\check{\phi}^T (\mathbf{L}^T \check{\phi} - \mathbf{G}^{\mathbf{T}} \gamma) \Big] \mathbf{dt} = \mathbf{0}. \tag{2.91}$$

The application of the fundamental lemma yields three matrix equations,

$$\underline{\underline{\mathbf{N}}}\, \underline{\ddot{\gamma}} + \underline{\underline{\mathbf{F}}}\, \underline{\gamma} - \underline{\underline{\mathbf{G}}}\, \underline{\check{\psi}} = \mathbf{0} \qquad \text{on} \qquad \Gamma, \tag{2.92}$$

$$\underline{\underline{\mathbf{L}}}^{\mathbf{T}} \underline{\check{\psi}} - \underline{\boldsymbol{f}} = \mathbf{0} \qquad \text{on} \qquad \Gamma_\psi, \tag{2.93}$$

$$\underline{\underline{\mathbf{L}}}\, \underline{\check{\phi}} - \underline{\underline{\mathbf{G}}}^{\mathbf{T}} \underline{\gamma} = \mathbf{0} \qquad \text{on} \qquad \Gamma, \tag{2.94}$$

From (2.94), it can be obtained the relation between the generalized loads $\underline{\gamma}$ and the nodal potentials $\underline{\phi}$. Since the matrices are time-invariant, the second time derivative is

$$\underline{\underline{\mathbf{L}}}\,\ddot{\underline{\phi}} - \underline{\underline{\mathbf{G}}}^{\mathbf{T}}\ddot{\underline{\gamma}} = 0, \tag{2.95}$$

Solving (2.94) and (2.95) for $\underline{\gamma}$ and $\ddot{\underline{\gamma}}$, respectively, yields relations for the generalized loads and their second time derivative as

$$\underline{\gamma} = (\underline{\underline{\mathbf{G}}}^{\mathbf{T}})^{-1}\underline{\underline{\mathbf{L}}}\,\check{\underline{\phi}} = \underline{\underline{\mathbf{R}}}\,\check{\underline{\phi}}; \quad \ddot{\underline{\gamma}} = \underline{\underline{R}}\,\ddot{\underline{\phi}}. \tag{2.96}$$

Inserting the last two equations into (2.92) , solving for $\check{\psi}$ and inserting in (2.93) leads to the equation of motion

$$\underline{\underline{\mathbf{M}}}\,\ddot{\underline{\phi}} + \underline{\underline{\mathbf{K}}}\,\check{\underline{\phi}} = \underline{\boldsymbol{f}}, \tag{2.97}$$

with the symmetric and positive-definite mass matrix

$$\underline{\underline{\mathbf{M}}} = \underline{\underline{\mathbf{L}}}^{\mathbf{T}}\underline{\underline{\mathbf{G}}}^{-\mathbf{1}}\underline{\underline{\mathbf{N}}}(\underline{\underline{\mathbf{G}}}^{-\mathbf{1}})^{\mathbf{T}}\underline{\underline{\mathbf{L}}} = \underline{\underline{\mathbf{R}}}^{\mathbf{T}}\underline{\underline{\mathbf{N}}}\,\underline{\underline{\mathbf{R}}}, \tag{2.98}$$

and the symmetric stiffness matrix

$$\underline{\underline{\mathbf{K}}} = \underline{\underline{\mathbf{L}}}^{\mathbf{T}}\underline{\underline{\mathbf{G}}}^{-\mathbf{1}}\underline{\underline{\mathbf{F}}}(\underline{\underline{\mathbf{G}}}^{-\mathbf{1}})^{\mathbf{T}}\underline{\underline{\mathbf{L}}} = \underline{\underline{\mathbf{R}}}^{\mathbf{T}}\underline{\underline{\mathbf{F}}}\,\underline{\underline{\mathbf{R}}}. \tag{2.99}$$

As stated in [5] the main diagonal of the matrix $\underline{\underline{\mathbf{F}}}$ is hypersingular and can be computed by assuming a constant potential distribution. By taking the first derivative of (2.97), we can obtain a pressure-flux ($p, q = \frac{\partial p}{\partial n}$) formulation,

$$\underline{\underline{\mathbf{M}}}\,\ddot{\underline{\mathbf{p}}} + \underline{\underline{\mathbf{K}}}\,\check{\underline{\mathbf{p}}} = \underline{\mathbf{q}} \qquad \text{with} \qquad \underline{\mathbf{q}} = \rho_{\mathbf{0}}\dot{\underline{\boldsymbol{f}}}. \tag{2.100}$$

This formulation can be extended to analyze problems with acoustic fluid-structure interaction in the time domain as explained by *Gaul, Kögl and Wagner (2003)*. It is important to remark that due to the lack of information on the Virtual.Lab manual this method is explained and recommended because of the advantages that will be explained in the following section, i.e. it is not implied that Virtual.Lab uses this method to solve acoustics problems in the time-domain.

Hybrid Displacement acoustic example

A 2-D steady-state acoustic example in a rectangular domain is performed in order to prove the advantages of the Hybrid Displacement Boundary Element Method over the Direct BEM. But first an analytical solution will be sought.

For the time-harmonic behavior the pressure p in an acoustic field is governed by the Helmholtz equation

$$\Delta^2 p(x) + \kappa^2 p(x) = 0, \qquad where \qquad \kappa = w/c. \tag{2.101}$$

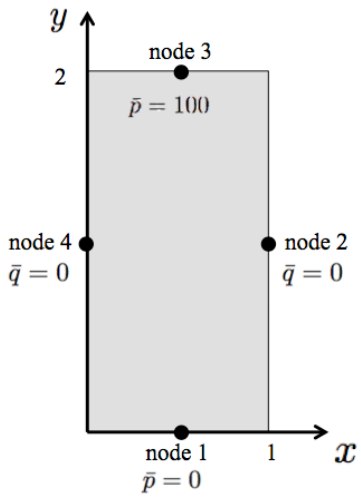

Figure 2.5.: Example of acoustics for the HDBEM

The acoustic flux q on the boundary is prescribed as

$$q(x) := \frac{\partial p(x)}{\partial n}, \qquad x \quad \epsilon \quad \Gamma. \tag{2.102}$$

In some applications like in the acoustics of a ship hull, the Helmholtz equation fades into a Laplace's equation by considering high sound velocities c and low frequencies of excitation w. In this way the wave number $\kappa \to 0$.

As shown in Figure 2.5 the domain of the problem has a ratio of 2:1. At the horizontal boundaries $y = const$ the acoustic pressures $p = \bar{p}$ are prescribed, while at the vertical boundaries the acoustic fluxes vanish.

In this example, our Laplace equation only depends on y, so it yields

$$\Delta p = 0 \to \cancel{\frac{\partial^2 p}{\partial x^2}} + \frac{\partial^2 p}{\partial y^2} = 0. \tag{2.103}$$

Solving the previous equation

$$p(y) = ay + b, \tag{2.104}$$

and substituting the boundary conditions into (2.104), we have

$$\begin{aligned} p(0) = 0 \quad &\to \quad b = 0. \\ p(2) = 100 \quad &\to \quad a = 50. \end{aligned}$$

Replacing the value of the constants a and b into (2.104) yields

$$p(y) = 50y. \tag{2.105}$$

Now the acoustic flux will be

$$q = \frac{\partial p}{\partial n} = \nabla p.\vec{n} = 50\vec{e}_y.\vec{n}. \tag{2.106}$$

Imposing the boundary conditions to obtain the expression for acoustic flux, we have

$$q_(y = 0) = 50\vec{e}_y.(-\vec{e}_y) = -50 \qquad q(y = 2) = 50\vec{e}_y.(\vec{e}_y) = 50 \tag{2.107}$$

Finally the unknown values of the pressure and acoustic pressure at the nodes are the following

$$p_2 = 50; \qquad p_4 = 50; \qquad q_1 = -50; \qquad q_3 = 50. \tag{2.108}$$

Continuing with the example, the domain is discretized with 4 elements with constant shape functions and $\bar{p}_1 = 0$, $\bar{p}_3 = 100$ and $\bar{q}_2 = \bar{q}_4 = 0$. The Hybrid Displacement Boundary Element Method (HDBEM) will be used to obtain the unknown values.

As explained in the previous section, the problem in a matrix notation can be stated as

$$.\mathbf{K}\begin{bmatrix} \bar{p}_1 \\ p_2 \\ \bar{p}_3 \\ p_4 \end{bmatrix} = \begin{bmatrix} f_1 \\ \bar{f}_2 \\ f_3 \\ \bar{f}_4 \end{bmatrix}. \tag{2.109}$$

First, the matrix $\mathbf{G}$ is computed according to equation(2.89). So we have

$$\underline{\underline{\mathbf{G}}} = \lim_{\varepsilon \to 0} \int_{\Gamma`} \underline{\phi}^* \underline{\underline{\Phi}}^{*^T} d\Gamma = \sum_{e=1}^{E} \left(\int_{\Gamma^{(e)}} -\frac{1}{2\pi} \ln|x - \varepsilon^l| d\Gamma \right) \tag{2.110}$$

where the super indices l and e stand for the load point and the element number respectively. By collocating the load point ε^l sequentially on all four nodes of the discretisation, we obtain four equations for the four unknown boundary values.

First, we calculate the matrix components G_{11} and G_{12}. We collocate the load point on node 1 and carry out the integration along the element 1 and 2 respectively, as shown in Figure 2.6.

$$G_{11} = -\frac{1}{2\pi} \int_0^1 \ln|x - 1/2| dx = 0.26947 \tag{2.111}$$

$$G_{12} = -\frac{1}{2\pi} \int_0^2 \ln \sqrt{(1/4 + y^2)} dy = -0.01748 \tag{2.112}$$

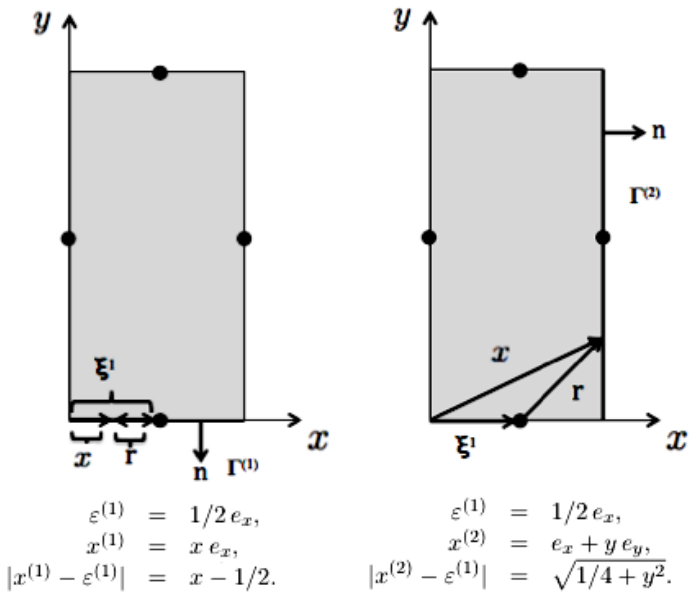

Figure 2.6.: Calculation of matrix elements G_{11} (left) and G_{12} (right)

The rest of the terms of the G matrix are obtained following the same procedure as the first two terms. The complete matrix yields

$$\mathbf{G} = \begin{bmatrix} 0.26947 & -0.01748 & -0.11194 & -0.01748 \\ -0.02100 & 0.31831 & -0.02100 & -0.04201 \\ -0.11194 & -0.01748 & 0.26947 & -0.01748 \\ -0.02100 & -0.04201 & -0.02100 & 0.31831 \end{bmatrix} \tag{2.113}$$

The next step is to compute the matrix $\mathbf{L}$ according to equation(2.90). This matrix only depends on the geometrical configuration since it only depends on the shape functions that describe both potential fields. In this case $\Phi_p = \Phi_q = \Phi = 1$. The integral for the elements 1 and 2 are

$$L^{(1)} = \int_{\Gamma^{(e)}} \Phi\Phi^T d\Gamma = \int_0^1 1 J dx = 1, \tag{2.114}$$

$$L^{(2)} = \int_{\Gamma^{(e)}} \Phi\Phi^T d\Gamma = \int_0^2 1 J dx = 2. \tag{2.115}$$

The global matrix $\mathbf{L}$ is formed by adding the results of each element according to the

global numbers of the load points.

$$\mathbf{L} = \begin{bmatrix} 1 & 0 & 0 & 0 \\ 0 & 2 & 0 & 0 \\ 0 & 0 & 1 & 0 \\ 0 & 0 & 0 & 2 \end{bmatrix}. \tag{2.116}$$

Then we can obtain $\mathbf{R}$ with the results $\mathbf{G}$ and $\mathbf{L}$.

$$\mathbf{R} = (\mathbf{G}^T)^{-1}\mathbf{L} = \begin{bmatrix} 4.59574 & 0.99864 & 1.97389 & 0.99864 \\ 0.41562 & 6.5209 & 0.41562 & 0.97030 \\ 1.97389 & 0.99864 & 4.59574 & 0.99864 \\ 0.41562 & 0.97030 & 0.41562 & 6.52092 \end{bmatrix}. \tag{2.117}$$

The hermitian matrix $\mathbf{F}$ couples the weakly and strongly singular fundamental solutions at the load points i and j and is calculated according to equation (2.89).

$$\mathbf{F}_{ij} = \sum_{i=1}^{4} \lim_{\varepsilon \to 0} \int_{\theta=0}^{\pi} p^*(x, \xi^{(i)}) q^*(x, \xi^{(j)}) \varepsilon d\theta + \sum_{e=1}^{4} \lim_{\varepsilon \to 0} \int_{\Gamma^{(e)\prime}} p^*(x, \xi^{(i)}) q^*(x, \xi^{(j)}) d\Gamma, \tag{2.118}$$

where the first sum of integrals is the contribution of the $i = 1, ..., 4$ small circles that exclude the load points from the domain. This integral is already transformed in polar coordinates. The second term contains the contributions of the modified domain. The needed expressions for field points, normals, and load points in order to compute the term F_{12} are

$$\begin{aligned} \vec{x}^{(1)} &= \begin{bmatrix} x \\ 0 \end{bmatrix}, \quad \vec{x}^{(2)} = \begin{bmatrix} 1 \\ y \end{bmatrix}, \\ \vec{n}^{(1)} &= \begin{bmatrix} 0 \\ -1 \end{bmatrix}, \quad \vec{n}^{(2)} = \begin{bmatrix} 0 \\ 1 \end{bmatrix}, \quad \vec{n}^{(3)} = \begin{bmatrix} 1 \\ 0 \end{bmatrix}, \quad \vec{n}^{(4)} = \begin{bmatrix} 0 \\ 1 \end{bmatrix}, \\ \vec{\xi}^{(1)} &= \begin{bmatrix} 0.5 \\ 0 \end{bmatrix}, \quad \vec{\xi}^{(2)} = \begin{bmatrix} 1 \\ 1 \end{bmatrix}, \quad \vec{\xi}^{(3)} = \begin{bmatrix} 0.5 \\ 2 \end{bmatrix}, \quad \vec{\xi}^{(4)} = \begin{bmatrix} -1 \\ 0 \end{bmatrix}, \end{aligned}$$

As explained in *Gaul, Kögl and Wagner (2003)* for constant elements, we have for the first term

$$F_{12}^{\varepsilon} = \frac{1}{2} p^*(\xi^{(1)}, \xi^{(2)}) = -\frac{1}{4\pi} \ln|\xi_i^{(1)} - \xi_i^{(2)}| = -\frac{1}{4\pi} \ln \sqrt{1 + 0.5^2} = -0.00888. \tag{2.119}$$

Now for the second term we calculate the contribution of each element separately in the following way

$$F_{12}^{(1)} = \frac{1}{4\pi^2} \int_{\Gamma'} \ln r^{(1)} \frac{r^{(2)} n^{(1)}}{r^{(2)^2}} d\Gamma = \frac{1}{4\pi^2} \int_{0}^{1} \frac{\ln(x - 0.5)}{(x-1)^2 + 1} dx = -0.03394. \tag{2.120}$$

$$F_{12}^{(2)} = \frac{1}{4\pi^2}\int_{\Gamma'} \ln r^{(1)} \frac{r^{(2)} n^{(2)}}{r^{(2)^2}} d\Gamma = \frac{1}{4\pi^2}\int_0^2 \frac{\ln\sqrt{y^2+0.5^2}(0)}{(y-1)^2} dx = 0. \tag{2.121}$$

$$F_{12}^{(3)} = \frac{1}{4\pi^2}\int_{\Gamma'} \ln r^{(1)} \frac{r^{(2)} n^{(3)}}{r^{(2)^2}} d\Gamma = \frac{1}{4\pi^2}\int_1^0 \frac{\ln\sqrt{(x-0.5)^2+2^2}}{(x-1)^2+1} dx = 0.01399. \tag{2.122}$$

$$F_{12}^{(4)} = \frac{1}{4\pi^2}\int_{\Gamma'} \ln r^{(1)} \frac{r^{(2)} n^{(4)}}{r^{(2)^2}} d\Gamma = \frac{1}{4\pi^2}\int_2^0 \frac{\ln\sqrt{y^2+0.5^2}}{(y-1)^2+1} dx = 0.00251. \tag{2.123}$$

$$F_{12} = F_{12}^{\varepsilon} + F_{12}^{(1)} + F_{12}^{(2)} + F_{12}^{(3)} + F_{12}^{(4)} = -0.02632 \tag{2.124}$$

To compute the main diagonal of $\mathbf{F}$ which contains hyper-singular entries, we use the following formula

$$F_{ii} - \frac{1}{r_i}\sum_{n=1;n\neq i}^{N} F_{in} r_n. \qquad where \qquad r = \mathbf{R}\begin{bmatrix}1 & 1 & 1 & 1\end{bmatrix}^T. \tag{2.125}$$

Following the same procedure for the rest of the terms, we have our complete $\mathbf{F}$ matrix

$$\mathbf{F} = \begin{bmatrix} 0.10064 & -0.02632 & -0.04950 & -0.02632 \\ -0.02632 & 0.09450 & -0.02632 & -0.04031 \\ -0.04950 & -0.02632 & 0.10064 & -0.02632 \\ -0.02632 & -0.04031 & -0.02632 & 0.09450 \end{bmatrix}. \tag{2.126}$$

Finally, after computing all the matrices, we obtain the symmetric stiffness matrix of our system according to (2.99).

$$\mathbf{K} = \begin{bmatrix} 1.35089 & -0.83479 & 0.31882 & -0.83479 \\ -0.83479 & 2.91164 & -0.83479 & -1.24178 \\ 0.31882 & -0.83479 & 1.35089 & -0.83479 \\ -0.83479 & -1.24178 & -0.83479 & 2.91164 \end{bmatrix}. \tag{2.127}$$

To be able to solve (2.109), the vector of equivalent nodal forces on each element is computed.

$$f^{(e)} = \int_{\Gamma^{(e)}} \Phi_1 \bar{q} d\Gamma = \int_0^1 \bar{q} J dx. \tag{2.128}$$

The complete vector $\boldsymbol{f}$ yields

$$\boldsymbol{f} = \begin{bmatrix} f_1 & 0 & f_3 & 0 \end{bmatrix}^T. \tag{2.129}$$

The solution applying HDBEM is

$$\begin{bmatrix} f_1 \\ p_2 \\ f_3 \\ p_4 \end{bmatrix} = \begin{bmatrix} -51.58300 \\ 49.99162 \\ 51.62400 \\ 49.99162 \end{bmatrix}. \tag{2.130}$$

Comparing these results with the ones obtained with Direct BEM (See *Gaul, Kögl and Wagner (2003)*)

$$\begin{bmatrix} q_1 \\ p_2 \\ q_3 \\ p_4 \end{bmatrix} = \begin{bmatrix} -75.77 \\ 50.00 \\ 75.77 \\ 50.00 \end{bmatrix}, \tag{2.131}$$

and the analytical results (2.108), we can see that the HDBEM gives much better results for this problem even with this coarse discretisation than the Direct BEM.

2.4.3. Numerical consistency factors

Virtual Lab requests the following values for any Time-domain simulation. According to [2], we define,

- **The Relaxation Factor** is a parameter that allows to fix the simulation time in a very intuitive way rather than in absolute time or number of time steps. It follows the following formula

$$T_{\text{simul}} = T_{\text{signal}} + \underbrace{\text{Relaxation Factor} \cdot \text{diam(object)} \ /c}_{T\text{relax}}, \tag{2.132}$$

  where T_{simul} is the simulation time duration; T_{signal} the time duration of the excitation signal and T_{relax} the relaxation time given.

- **The Courant Friedrichs Levy (CFL)** is defined as $CFL = c \cdot \Delta t/h$, where c is the speed of sound, Δt is the time step and h is the mesh size. The mesh size h corresponds to the maximum of the element diameters.

  The Virtual.Lab BEM time solver is said to be unconditionally stable i.e. it is always stable, independently of the value of the *CFL*. Nevertheless, even if always stable, the accuracy will still depend on the value of the *CFL*. The smaller it is, the higher the precision will be but also the more expansive the computation will be (both in terms of CPU and memory). In most cases – for a good trade-off between accuracy and cost – a *CFL* should be between 0.2 and 2.

- **FASTLVL** represent the optimization level of the convolution. The higher the value of *FASTLVL* will be, the higher the optimization will be. The highest gain will be observed for high values of the relaxation factor.

2.5. Signal Processing

Any pressure-time history (even isolated transients) maybe mathematically decomposed into, or constructed from, an infinite number of sinusoids of infinite duration (Fourier Theorem) [4]. The amplitudes and phases of the sinusoids are determined by the specific time history. The distributions of the amplitudes and phases as functions of frequency are termed the *amplitude and phase spectra*.

Periodic sounds, such as compressor whines or regularly repeated impacts, have spectra which only have non-zero components at discrete frequencies which are multiples of the fundamental frequency, which is the inverse of the event period. These are called "*line spectra*". On the other hand, aperiodic sounds, such as isolated impacts, have continuous frequency spectra.

Frequency analysis of sound is very important in acoustics and vibration for the following reasons:

1. the sensitivity of human auditory system and the vibrational response of mechanical systems to sound is frequency dependent.

2. the performance of a noise control system varies with frequency.

3. the mathematical analysis of sinusoidal sound is relatively straightforward, and any sound field and its effects may be synthesized by the addition of harmonic components.

The **spectral analysis** is then performed either by the use of contiguous filters or by the Fourier analysis via the *Discrete Fourier Transform* (DFT), which is conventionally implemented by various algorithms which are collectively described as *Fast Fourier Transforms* (FFT).

2.5.1. Fast Fourier Transform (FFT)

In Acoustics, next to the periodic signals, non-periodic signals are also found relatively often in everyday practice. Transient phenomena and mechanical shocks are represented by these signals. They may be defined in terms of force, acceleration, velocity or displacement and for a complete description it is necessary to obtain an exact time history record of the quantity in question. In many cases the ultimate goal is not the waveform itself, but rather a means to estimate the effect that the corresponding shock or transient vibration would have on a certain mechanical system. A more useful method of description might be found in the form of Fourier analysis.

If the time function for a shock is $f(t)$ then its Fourier transform is given by

$$F(f) = \int_{-\infty}^{\infty} f(t)e^{-jwt}dt, \tag{2.133}$$

The Fourier transformed $F(f)$ is clearly interpreted as an infinite overlay from multiple vibrations with continuously lined up frequency w and its corresponding 'Amplitudes' $F(f)$. Thus $F(f)$ is the complex spectral amplitude density from the given function $f(t)$. If t is interpreted as time, then w takes the form of the angular frequency or frequency. If t is treated as a space coordinate, then w is taken as the wavelength number.

In order for the Fourier Transformation to take place, the function $f(t)$ must meet the following conditions:

1. $f(t)$ must be a smooth function by parts. Only finite discontinuity points are allowed.

2. The integral over $f(t)e^{-jwt}$ must exist.

The **FFT** operation transforms discrete (i.e. sampled) signals from the time domain into the frequency domain. The frequency domain values express how the time signal is composed of a sum of different waves, each with their own amplitude and phase. Each sine wave in the time domain is represented by one spectral line in the frequency domain. The series lines describing a waveform is known as its frequency spectrum. For a deeper understanding on this topic, the reader should consult [3].

2.5.2. Windowing / Leakage

A **window function** (also known as apodization function or tapering function) is a mathematical function that is zero-valued outside of some chosen interval. One of the basic assumptions of the Fourier Transform is that the time domain signal repeats itself. In practice, this is often not the case, because the selected time segment is finite, and it is not possible to select a part of the signal that is exactly repetitive. The signal is typically windowed before performing the FFT in order to avoid that abrupt difference between the last part of the signal and the first part (which are assumed to connect seamlessly).

The use of windows gives rise to errors itself of which the user should be aware and should be avoided if possible.The leakage is one of this errors and is defined as the non-zero values that develop at frequencies other than the frequency of our signal if we consider a simple sinusoidal one. The various types of windowing functions distribute the energy in different ways. The choice of window can play an important role in determining the quality of overall results.

The windows vary in the amount of energy squeezed into the central lobe as compared to that in the side lobes. The selection of window depends on both the aim of the analysis and the type of signal. In general the broader the noise bandwidth, the

worse the frequency resolution, since it becomes more difficult to pick out adjacent frequencies with similar amplitudes (see Figure 2.7 . On the other hand, selectivity (i.e. the ability to pick out a small component next to a large one) is improved with side lobe fall off. It is typical that a window that scores well on bandwidth is weak on side lobe fall off and the choice is therefore a trade off between the two. A summary of these characteristics of the windows is provided in Table (2.2) extracted from [2]

Table 2.2.: Properties of time windows

Windows type	Highest side lobe (dB)	Sidelobe falloff (dB/decade)	Noise Bandwidth (bins)	Correction Factors	
				Amplitude	Energy
Uniform	-13	-20	1.00	1	1
Hanning	-32	-60	1.50	2	1.63
Hamming	-43	-20	1.38	1.85	1.59
Kaiser-Bessel	-69	-20	1.80	2.49	1.86
Blackman	-92	-20	2.00	2.80	1.97
Flattop	-93	0	3.43	4.18	2.26

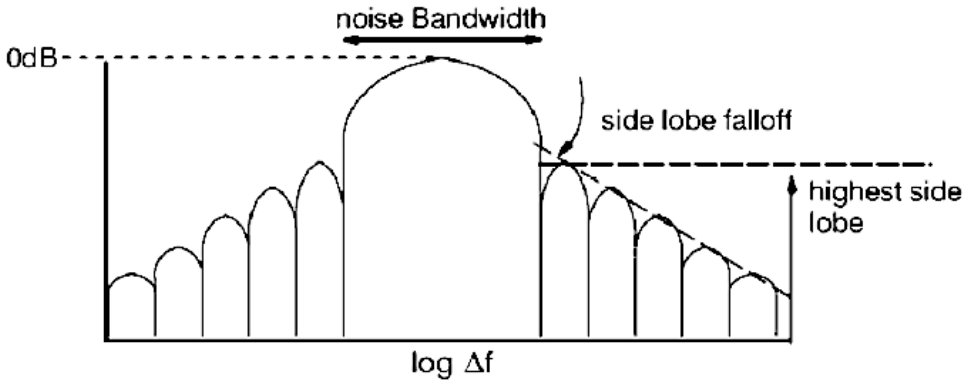

Figure 2.7.: Characteristics of windows in frequency domain

The most common types of windows will be briefly described.

- **Uniform Window**.

  Also known as **Rectangular window** is used when leakage is not a problem since it does not affect the energy distribution. It is applied in the case of periodic sine waves, impulses, and transients, where the function is naturally at the start and end of the sampling period.

- **Hanning Window**.

  This window is most commonly applied for general purpose analysis of random signals with discrete frequency components. It has the effect of applying a round topped filter. The ability to distinguish between adjacent frequencies of

similar amplitude is low so it is not suitable for accurate measurements of small signals

- **Hamming Window**.

  This window has a higher side lobe that the Hanning but a lower fall off rate and is best used when the dynamic range is about 50dB.

- **Blackman Window**.

  This window is useful for detecting a weak component in the presence of a strong one.

- **Kaiser-Bessel Window**.

  The filter characteristics of this window provide good selectivity, and thus make it suitable for distinguishing multiple tone signals with widely different levels. It can cause more leakage than a Hanning window when used with random excitation.

- **Flattop Window**.

  This window's name derives from its low ripple characteristics in the filter pass band. This window should be used for accurate amplitude measurements of single tone frequencies and is best suited for calibration purposes.

3. Numerical Examples

In order to check the liability of the acoustic study performed in transient BEM in Virtual.Lab (VL), two examples were selected and simulated in both VL and ABAQUS. The methodology used to compute the acoustic results will be explained in this section.

3.1. Zero-order monopole

For the case of the monopole, transient acoustic simulations were performed within the hearing range (2-20 kHz) with intervals of 2 kHz. The monopole radius is set to be $10mm$ and the displacement amplitude $1mm$.

The acoustic properties of this problem are shown in Table (3.1).

Table 3.1.: Acoustic properties for the air.

Density ρ (kg/m^3)	Sound velocity c_{air} (m/s)	Bulk modulus K (Pa)
1.225	340	141610

3.1.1. FEM Computations

In ABAQUS, since we are dealing with a finite element software, there is the need to model the monopole surface and the surrounding acoustic medium. A fully coupled system is taken into account where the surface displacements of the monopole are controlled as our input excitation and as the output variable we are interested in the acoustic pressure.

In Table (3.2), there is a summary of the values of wavelength λ, minimum distance between the non-reflecting boundary condition and the surface of the radiator d_b, the time period T, the time step Δt and the total time t_{total}. The total time and time step were computed after $t_{\text{total}} = T \cdot 30$, and $\Delta t = T/12$ respectively. These formulas were arranged in this way in order to have enough sinusoidal waves with good resolution allowing to perform an optimum analysis.

To facilitate the task of simulating this wide range of frequencies, three different acoustic meshes were modeled in ABAQUS to avoid the computation of unnecessary values in the far field, thus saving computational time. The parameters that rule the

geometry of the meshes are highlighted in Table (3.2) and the discretization of these three groups are shown in Figure 3.1.

Table 3.2.: Monopole frequencies

Frequency $f(Hz)$	Wavelength $\lambda(m)$	Distance $d_b(m)$	Period $T(s)$	Time step $\Delta t(s)$	Time $t_{total}(s)$
2000	0.17	**0.255**	0.0005	4.1667e-5	0.015
4000	0.085	0.1275	0.00025	2.0833e-5	0.0075
6000	**0.05667**	0.085	0.000167	1.3889e-5	0.005
8000	0.0425	**0.06375**	0.000125	1.0417e-5	0.0375
10000	0.034	0.051	0.0001	8.3333e-6	0.003
12000	**0.02833**	0.0425	8.33e-5	6.9444e-5	0.0025
14000	0.0243	**0.036429**	7.1429e-5	5.9524e-5	0.002143
16000	0.02125	0.031875	6.25e-5	5.2083e-5	0.001875
18000	0.0189	0.0283	5.556e-5	4.6296e-5	0.001667
20000	**0.017**	0.0225	5e-5	4.1667e-6	0.0015

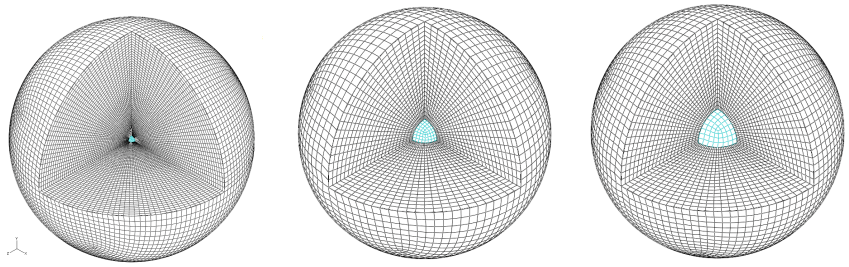

(a) (b) (c)

Figure 3.1.: Discretization of monopole source for FEM. a)2-6 kHz , b)8-12 kHz, c)14-20 kHz

In practice, non-reflecting radiation boundary conditions provide accurate results, when the surface is at a distance $d_b \geq 1.5\lambda$,where λ is the wavelength at the lowest frequency of interest. Therefore, the distance was selected as $d_b = 1.5\lambda$ following the equation (2.44). Besides, we have the rule of thumb that states that "the discretization requirements of the finite element method in wave problems require at least six nodes per wavelength" [1]. In this case the quantity of ten elements per the smallest wavelength of the group was chosen.

The three acoustic meshes with their geometry are specified in Table (3.3).

Table 3.3.: Geometry of acoustic meshes.

Group (kHz)	r_{ext} (mm)	h^* (mm)	Element type	Number of elements	Number of nodes
$2-6$	265	5.67	AC3D8	339300	346932
$8-12$	73.75	2.83	AC3D8	69000	72048
$14-20$	46.43	1.70	AC3D8	85764	89892

*the approximate global size

where the element AC3D8 is a linear acoustic tetrahedral element.

The monopole on the other hand has its geometric parameters listed in Table (3.4)

Table 3.4.: Geometry of structural mesh.

r (mm)	h^* (mm)	Element type	Number of elements	Number of nodes
10	2	S4R	384	386

*the approximate global size

The monopole is modeled as a shell structure with S4R elements, which are 4-node general-purpose shell elements and use reduced integration with hourglass control.

A *TIE constraint* (structure-fluid interaction) between the sphere and the acoustic medium is set, where the sphere is taken as the master surface and the acoustic medium as the slave surface.

For the displacements, a periodical signal is created by setting the amplitude to *periodic* type and introducing the respective values for each frequency, such as the *angular frequency* w, the *initial amplitude* A_0, the *starting time* t_0 and the parameters A_i and B_i, where $n = 1, 2, 3, \ldots N,$. The signal is obtained then after the formula:

$$a = \begin{cases} A_0 + \sum_{n=1}^{N} [A_n \cos nw(t-t_0) + B_n \sin nw(t-t_0)] & \text{for} \quad t \geq t_0, \\ A_0 & \text{for} \quad t < t_0, \end{cases}$$

With a displacement-type boundary condition and spherical coordinate system, the signal is assigned to the surface with an uniform distribution only in the radial direction ($U1$). The other 5 degrees of freedom are fixed with zero values. In this way, we obtain the proper conditions to model the behavior of the zeroth-order monopole.

Implicit dynamic analyses were performed for every frequency requesting as output history variables the acoustic pressure (POR) in points evenly distributed on the free field (external surface of the acoustic medium) as well as the displacements on the surface of the monopole. The time step introduced in the implicit analyses are the

ones from Table (3.2), which were selected small enough that they could sufficiently describe the wave.

3.1.2. BEM Computations

The simulations are run in the *transient BEM* module of Virtual.Lab. The next step is the creation of our BE acoustic mesh. FE meshes are generally not appropriate for acoustic radiation predictions because they contain too many elements and exhibit detailed features like holes, ribs and fillets which might not be relevant for the case.

VL offers a module called *Mesh coarsening*. This module allows us to create the acoustic BE mesh starting from an imported structural finite element mesh. The procedure basically consists of:

- applying a *Skinning tool* that transforms the volume elements into surface elements;
- then a *fixing and cleaning tool* is to be applied, where interior nodes, 1D nodes and non-acoustic elements are eliminated. Superimposed nodes and elements are merged and the normal consistency on the elements is checked.
- Finally, the *wrapping tool* which creates a mesh that adapts to the previously skinned, fixed and cleaned structural FE mesh according to requested parameters like *Maximum frequency* to be used or the *element size*.

For the case of the monopole this tool does not change the shape but the density of the mesh because we are dealing with a smooth sphere which is perfectly suited for the acoustic simulation.

As well as in ABAQUS, three acoustic meshes with different densities were created in VL,. Giving the maximum frequency of each group and changing the default parameter of number of elements per wave to 10, we obtain the following geometrical parameters listed in Table (3.5) and the discretization can be seen in Figure 3.2. The 26 points, where the acoustic pressure is to be measured, were evenly distributed at a distance equal to the distance used in ABAQUS for its corresponding frequency as can be seen in Figure 3.3, where the vertices of the field point mesh sphere represent the microphones position and the surface is not relevant for the case.

Table 3.5.: Geometry of BE acoustic meshes.

Group (kHz)	$h_{max}{}^*$ (mm)	Element (mm)	Number of elements	Number of nodes
$2-6$	6.149	TRIA3	288	146
$8-12$	3.138	TRIA3	384	194
$14-20$	1.138	TRIA3	1212	608

*the maximum of the element diameters

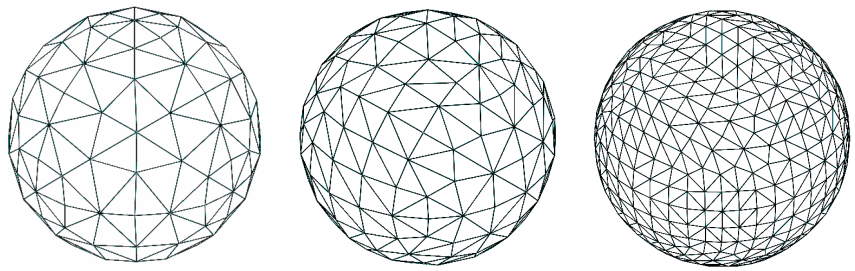

(a) (b) (c)

Figure 3.2.: Discretization of monopole source for BEM. a)2-6 kHz , b)8-12 kHz, c)14-20 kHz

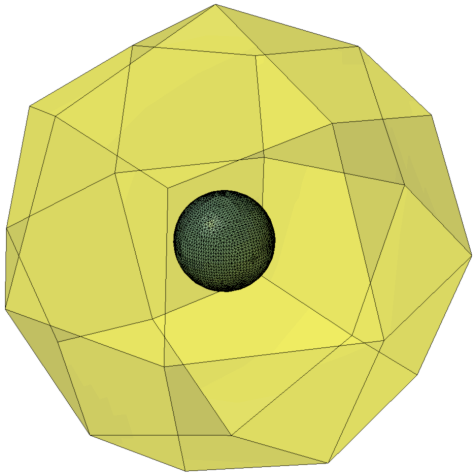

Figure 3.3.: Microphones layout in Virtual Lab

3.1.3. Sentitivity analysis

In Virtual.Lab, a sensitivity analysis of the acoustic mesh density was performed for the monopole in the frequency of 20 kHz.

The relevant data concerning the acoustic meshes used for this analysis is listed in Table (3.6). These meshes were created by entering different maximum frequencies in the *Mesh coarsening* module.

A transient IBEM analysis was performed with each acoustic mesh setting up the surface displacements as an input in our acoustic mesh by performing a mapping procedure that transfer nodal data from the structural FE mesh. In theory, the acoustic pressure of a zeroth-order monopole only depends on the radial distance when considering a spherical-coordinate system. Despite this fact, the acoustic pressures were requested in 26 evenly distributed points located at a radius equal to the exterior radius of the acoustic FE mesh, i.e, in the far field. In Figure 3.4 one can observe

Table 3.6.: Geometrical properties of the acoustic meshes used in the sensitivity analysis

Acoustic Mesh ID	Frequency (kHz)	Number of nodes	Number of elements	Element size (mm)
1	8	56	108	7.083
2	10	98	192	5.667
3	12	146	288	4.722
4	14	144	284	4.048
5	16	194	384	3.542
6	18	258	512	3.148
7	20	296	588	2.833
8	25	416	828	2.267
9	30	608	1212	1.889
10	35	770	1536	1.619
11	40	986	1968	1.417
12	50	1514	3024	1.133
13	60	2072	4140	0.944
14	70	2833	5662	0.810
15	80	3582	7160	0.708

from a zoom of the acoustic pressure plot that there is a small difference between the acoustic pressures measured at different points, therefore a mean value was computed out of these values. These differences can be attributed to the course discretization of the mesh.

From the Figure 3.5, we can see that the expected behavior was obtained. The higher the number of elements the smaller the relative error of the acoustic pressure. The recommended value by VL for our frequency is considered to be good and finer meshes do not entail improvements in the results.

3.1.4. Post-proccesing

Once the acoustic pressures are obtained in both methods, we begin the post-processing phase in Matlab. The steps taken in this procedure are the following:

- values are read and stored as matrices;
- if the time step is not constant, the values are interpolated to fit constant time steps;
- a hanning window is applied to the signal;
- a Discrete Fourier Transform is performed to obtain frequency-dependent acoustic pressures;

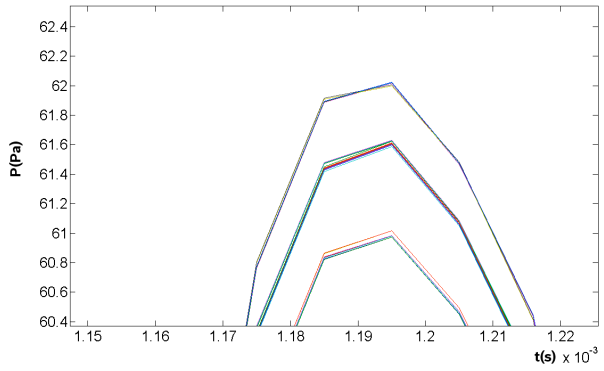

Figure 3.4.: BEM Acoustic pressure of monopole measured in different microphones for 2 kHz. Zoom of one peak

- the values are multiplied by the correction factors of the window and the Fourier Transform and the effective values of the pressure are computed;
- finally, it is possible to compute the sound pressure level. Subsequently with the structure-borne sound power, the radiation level is obtained.

The formulas used to obtain the radiation level starting from values in the frequency domain are the following [7]. First, we compute the *Structure-borne sound power level* L_K as

$$\begin{aligned} L_K(f) &= 10 \cdot \log_{10}(P_K(f)) = 10 \cdot \log_{10}\left[(\rho c)_{\text{air}} \int_S [v_n(f)]^2 dS\right] \\ L_K(f) &= 10 \cdot \log_{10}\left[(\rho c)_{\text{air}} \sum_{i=1}^{\text{nElem}} [v_{n,i}(f)]^2 \cdot \frac{S_i}{S_0}\right], \end{aligned} \tag{3.1}$$

where,

v_n → the normal velocity on the surface,
P_K → the structure-borne sound power,
S_i → the area of the element i,
S_0 → the reference area, $S_0 = 1m^2$, and
f → the frequency.

Then, for the *Sound power level*, we use

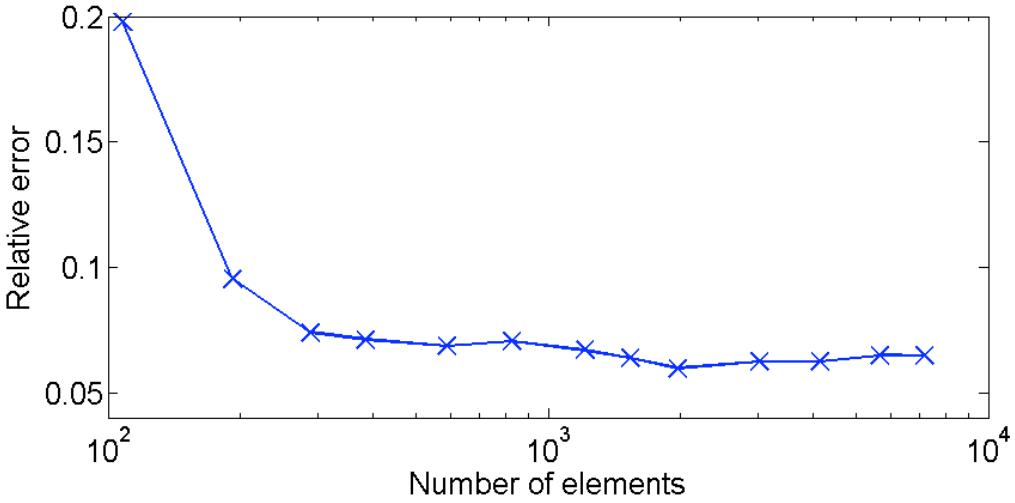

Figure 3.5.: Sensitivity plot. Number of elements vs Relative error

$$
\begin{aligned}
L_L(f) &= 10 \cdot \log_{10}(P_L(f)) = 10 \cdot \log_{10}\left[\oint_S \frac{1}{\rho c} p_{\text{eff}}^2 dS\right] \\
L_L(f) &= 10 \cdot \log_{10}\left[\frac{S_i}{S_0} \sum_{i=1}^{\text{nMic}} 10^{\{L_p^i(f)/10\}}\right], \\
L_p^i &= 10 \cdot \log_{10}\left(\frac{p_{\text{eff}}^2}{p_0^2}\right),
\end{aligned}
\tag{3.2}
$$

where

P_L → the sound power,
p_{eff} → the effective pressure,
S_i → the area of the element i,
S_0 → the reference area ($S_0 = 1\ m^2$), and
f → the frequency.

Finally, the radiation level is obtained through

$$
\sigma(f) = \frac{P_L(f)}{P_K(f)}, \qquad L_\sigma = 10 \cdot \log_{10}[\sigma(f)]. \tag{3.3}
$$

3.2. SOUND-RADIATING TUBE

This example is the simplification of the dynamics of an injection valve. It comprises an one-open ended tube which is impacted in the central axis by a rigid sphere causing the vibrations in the tube and thus sound is radiated to the surroundings..

Let the inner and outer diameter of the tube be 7 mm and 11 mm respectively, its length 65.45 mm, the ending cap thickness 2 mm and the diameter of the rigid sphere 2 mm with an initial velocity of 500 m/s in the negative direction of the Y axis .The tube is restricted with two bushings as seen in Figure 3.6.

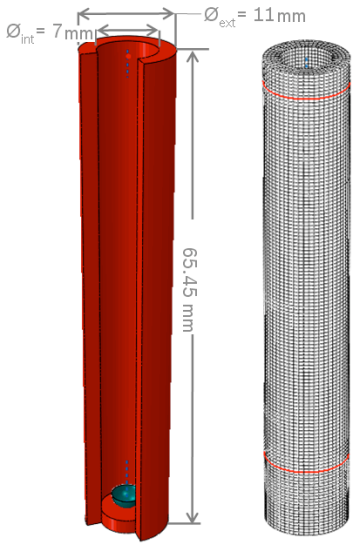

Figure 3.6.: Geometry (left) and bushing restrictions of the tube (right)

3.2.1. FEM Computations

The tube and acoustic medium are modeled in ABAQUS in the same way as for the monopole. The material properties of the tube and of the air are shown respectively in Tables (3.7) and (3.8).

Table 3.7.: Material properties for the tube.

Density ρ (t/mm^3)	Young's Modulus $E(MPa)$	Poisson's ratio ν
8.542e-9	25e3	0.3

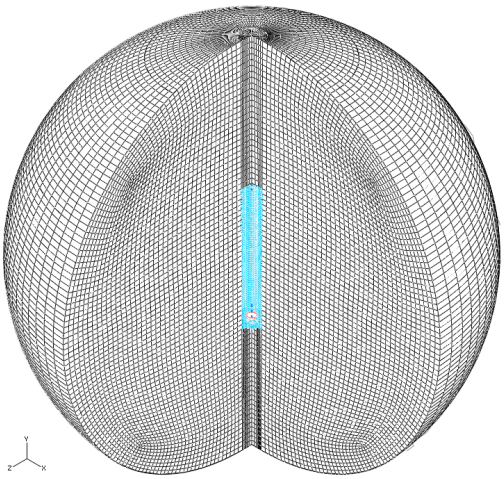

Figure 3.7.: Meshing of the tube and acoustic surrounding in FEM

Table 3.8.: Material properties for air.

Density ρ (t/mm^3)	Sound velocity c_{air} (mm/s)	Bulk modulus K (MPa)
1.225e-12	3.40e5	0.141610

Regarding the meshing of the problem, the tube meshing properties can be found in Table (3.9).

Table 3.9.: Geometry of structural mesh of the tube.

h^* (mm)	Element type	Number of elements	Number of nodes
0.5	C3D8	40255	49056

*the approximate global size

The geometrical properties of the acoustic mesh on the other hand are summarized in Table (3.10).

Two different approaches, a *Fully coupled* and a *Sequentially coupled* simulation, were taken for this example. In both approaches, two cases were considered. One case, where the bottom surface radiation is taken into account and the other one where this phenomenon is neglected.

Table 3.10.: FE acoustic mesh properties.

h^* (mm)	Element type	Number of elements	Number of nodes
2.36	AC3D8R	279916	287496

*the approximate global size

In the *Fully coupled* approach, the whole domain is processed in a single simulation and the displacements are also affected by the surrounding air. The following conditions (see Figure 3.8) were introduced to reproduce this case:

- A non-reflecting radiation condition with a spherical impedance interaction is imposed in the exterior surface of the acoustic mesh to allow any wave to pass through and not reflect back to the acoustic domain.
- FSI-Tie constraints were imposed according to the case. The surface of the tube is selected to be the master surface and the air surface the slave.
- A coupling distributing constraint is applied to simulate the effect of the O-rings acting on the tube.
- A surface-to-surface interaction is set between the rigid sphere surface(master) and the bottom surface of the tube (slave). This interaction is a penalty-type contact with finite sliding assumption.
- In two points, located at both extremes of the tube, an encastre-type BC is imposed.
- All degrees of freedom but the vertical translation (U2) are restricted for the rigid sphere.

For the *sequentially-coupled* system case, the computational domain is divided into two parts. The *Global model*, which comprises the dynamic implicit analysis of the rigid sphere impact against the tube, and the *submodel*. In the former, the acoustic mesh is not modeled and therefore the surface displacements of the tube are requested as output field request. These displacements are then entered as driven variables for the *submodel* case which also has the same boundary conditions as the fully coupled system applied to the acoustic mesh.

In order to compute the structure-borne sound, a series of 20 points, where velocities are requested as history output, were located on the external cylindrical surface of the tube at different values of Y for the *global model* (see Figure 3.9). These points were distributed exactly on the XY- and ZY plane. Therefore, the ones on the XY plane would have the normal velocity in the x-direction and the ones on the ZY plane in the z-direction. Besides, the y-direction of the four points on the bottom were taken for the velocities of the bottom surface. An assumption is taken into

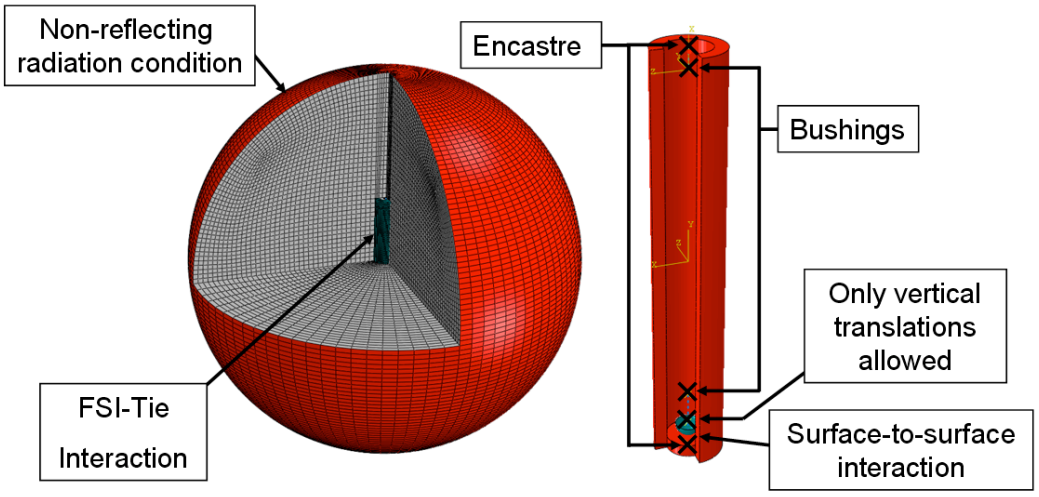

Figure 3.8.: Zeroth-order Monopole

account in which the normal velocities at each point represent the velocity of equally divided portions of the surface.

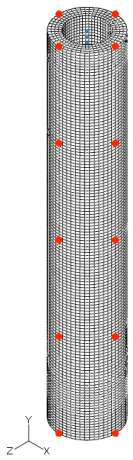

Figure 3.9.: Layout of 20 points where normal velocities are requested

3.2.2. BEM Computations

The *sequentially-coupled* system was computed in the transient IBEM module. The acoustic medium properties are the same as the ones used for the FEM approach. The FE structural mesh is imported into VL and the same procedure as in the monopole is applied, i.e., we get our BE acoustic mesh from the FE structural mesh in the *coarsening mesh* module (see Figure 3.10). As the maximum frequency criterion a

frequency of 40 kHz was entered and the resulting BE acoustic mesh geometrical properties are summarized in Table (3.11).

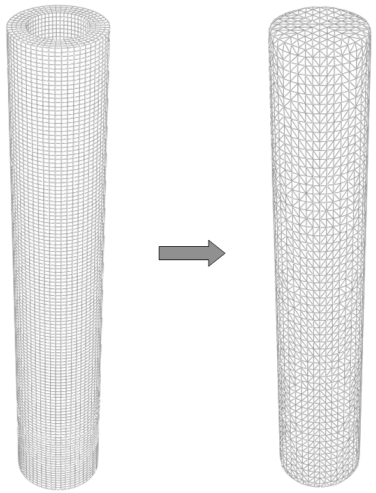

Figure 3.10.: Structural mesh imported from ABAQUS (left) and acoustic mesh (right) obtained in Virtual.Lab after processing the imported FEM mesh

Table 3.11.: BE acoustic mesh properties.

$h_{\max}{}^*$ (mm)	Element type	Number of elements	Number of nodes
1.562	TRIA3	4992	2498

*the maximum of the element diameters

The next step is the *mapping of the data*. The displacements obtained in the *global model* from ABAQUS are mapped into the acoustic mesh. In this step we include or neglect the bottom surface radiation of the tube. In order to do so, the following steps are performed:

- The acoustic mesh is divided into zones.
- As the source mesh, only the surfaces of interest are selected.
- Finally, the whole acoustic mesh is entered as the target mesh.

This way, the neglected surfaces (surfaces not included in the source mesh group) will have zero displacements in time assuring that no sound will be transmitted

through this surfaces. This procedure is analogous to the ABAQUS procedure of suppressing the FSI-Tie constraint on a surface.

The microphones layout used here is the same as the one in ABAQUS. The locations were entered as field point meshes.

3.2.3. Modal Analysis

A modal analysis of the tube with a Lanczos eigensolver was performed in ABAQUS requesting the eigenmodes in the range from 1-20 kHz. In such a problem involving a metal structure in contact with air, it is essential to compute the eigenmodes since these modes will usually dominate the behavior of the system.

3.2.4. Post-proccesing

As in the previous example, the whole post-processing was performed in Matlab. Therefore, all the results are exported to calculus sheets and read from Matlab.

The structure-borne sound power level is the first term to be computed. The normal velocities needed are taken from the *global model*, specifically from the series of 20 points that were collocated on the surface. After interpolating the values to constant time steps or verifying that this condition was met, a Fast-Fourier Transformation was applied in order to obtain frequency-dependent normal velocities. Then according to (3.1), the structure-borne sound power level is obtained.

Now, the sound power level is computed according to (3.2) with the previously transformed acoustic pressures into the frequency domain.

Finally, the radiation efficiency and radiation level can be computed according to Equation (3.3).

4. Results

The results obtained from the procedures performed in the previous chapter are presented in this section.

4.1. Monopole

4.1.1. Acoustic Pressures

The acoustic pressures obtained from both methods are compared in the Figures 4.1- 4.3 . In these figures, the blue curve is the input velocity signal of the monopole surface taken from the sinusoidal input displacements also set as boundary conditions in the surface of the monopole; the green curve displays the acoustic pressures obtained in ABAQUS and the magenta curve the ones obtained in Virtual.Lab.

As explained in the theory of the monopole, the acoustic pressure is directly proportional to the normal velocity. Hence the expected response to the velocity signal should present the same pattern but displaced in time so many seconds as it takes for the wave to travel from the surface to the microphone. Since we are working here with different group meshes, these times will vary according to the mesh group and they are summarized in the Table (4.1)

Table 4.1.: Analytical reaching time of wave according to meshgroup.

	Group I (2-6kHz)	Group II (8-12kHz)	Group III (14-20kHz)
time (s) x10^{-4}	7.5	1.875	1.071

The results from the two methods are similar. The difference lie in the response of the first peaks of the wave but after a while they both show the same pattern. For the FEM values the first peak response is either underestimated or neglected. This effect could be attributed to the numerical damping control parameter $\alpha = -0.05$, which allows the automatic time stepping procedure to work smoothly in ABAQUS.

The values of the acoustic pressures are also computed analytically according to (2.33). Then they are compared to the FEM and BEM values and are summarized in the Table (4.2). The pressure values listed correspond to the peak values.

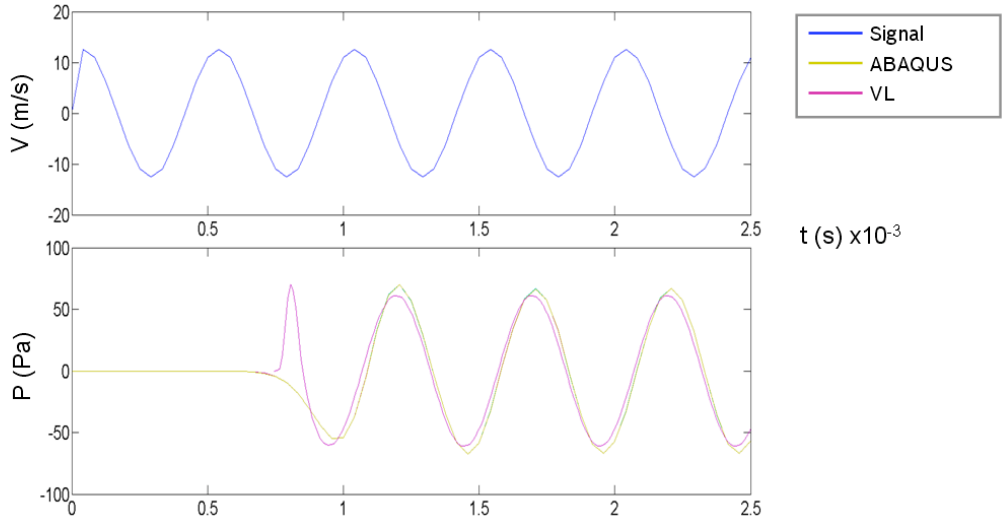

(a)

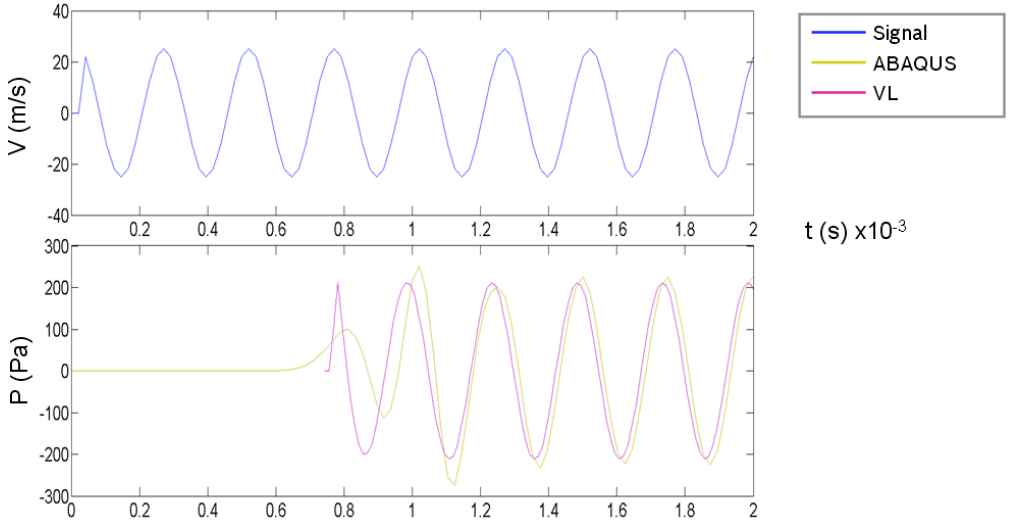

(b)

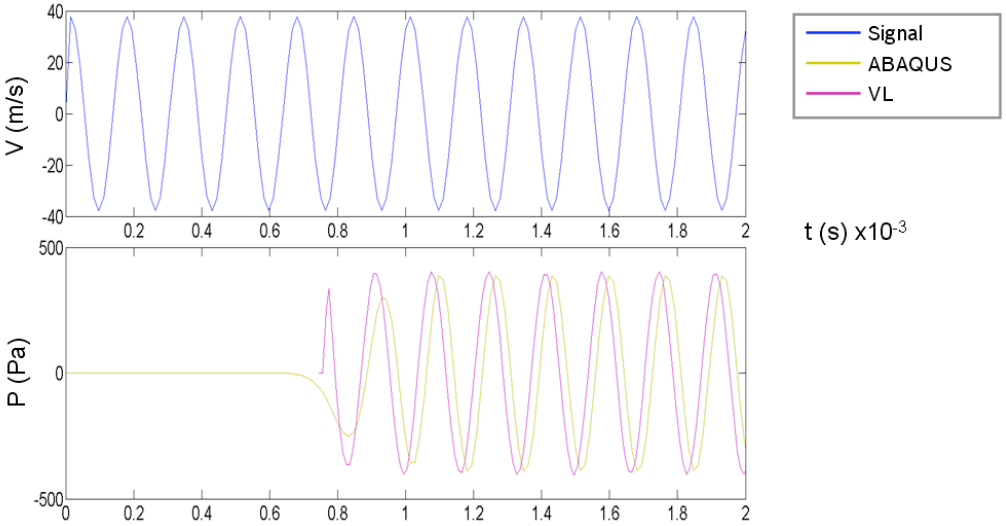

(c)

Figure 4.1.: Comparison of acoustic pressures obtained in BEM and FEM. a)$2kHz$, b)$4kHz$, c)$6kHz$

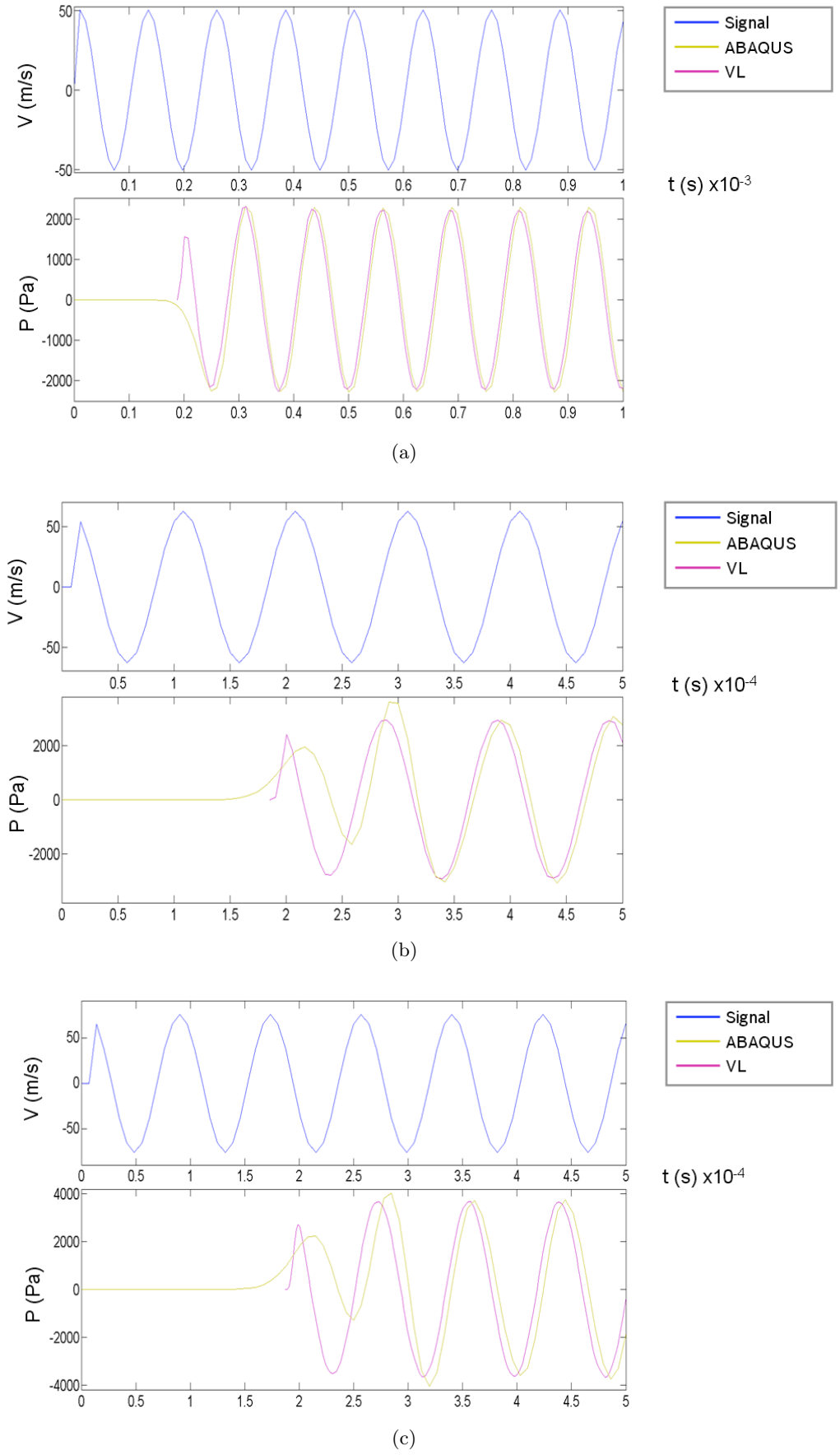

Figure 4.2.: Comparison of acoustic pressures obtained in BEM and FEM. a)$8kHz$, b)$10kHz$, c)$12kHz$

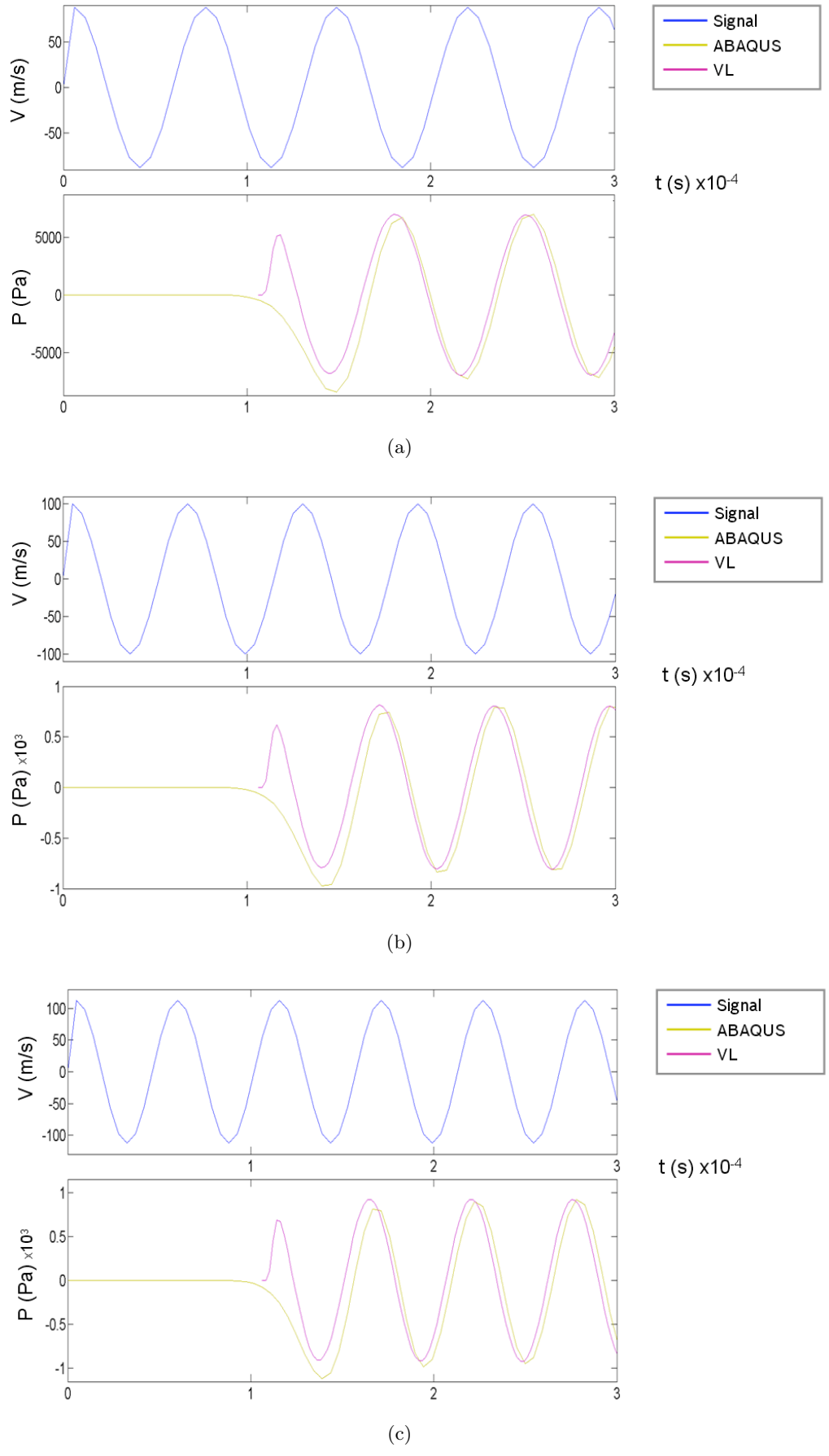

Figure 4.3.: Comparison of acoustic pressures obtained in BEM and FEM. a)$14kHz$, b)$16kHz$, c)$18kHz$

Table 4.2.: Summary of acoustic pressures of the monopole.

Frequency (kHz)	Analytical value (Pa)	FEM value (Pa)	BEM value (Pa)	FEM relative error (%)	BEM relative error (%)
2	69	67	62	1.8	9.9
4	235	226	212	3.7	6.6
6	440	381	403	13.5	8.3
8	2351	2299	2211	2.2	6.0
10	3121	3080	2929	1.3	6.1
12	3882	3765	3626	3.0	6.6
14	7360	7076	6920	3.9	6.0
16	8543	8391	8026	1.8	6.1
18	9716	9270	9132	4.6	6.0
20	10881	10462	10232	3.9	6.0

4.1.2. Radiation Efficiency

The radiation efficiency computed in the post-processing of both methods are compared with the analytical radiation efficiency (See Figure 4.4). It is important to keep in mind that we are working here with three different mesh densities as mentioned before.

It can be noted that the results in VL always underestimate the values with a smooth behavior while in ABAQUS the results oscillate around the analytical values. In the FEM results, as expected, the lower the frequency the better results we get for every mesh group. This is due to the fact that for lower frequencies we have a more refined mesh leading to more accurate results.

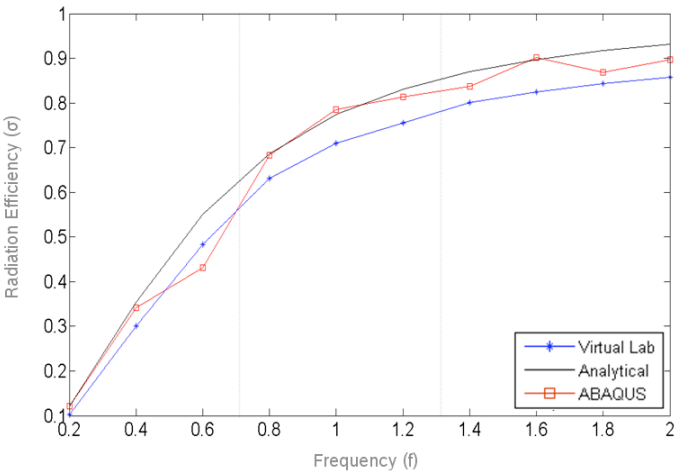

Figure 4.4.: Radiation efficiency of the monopole

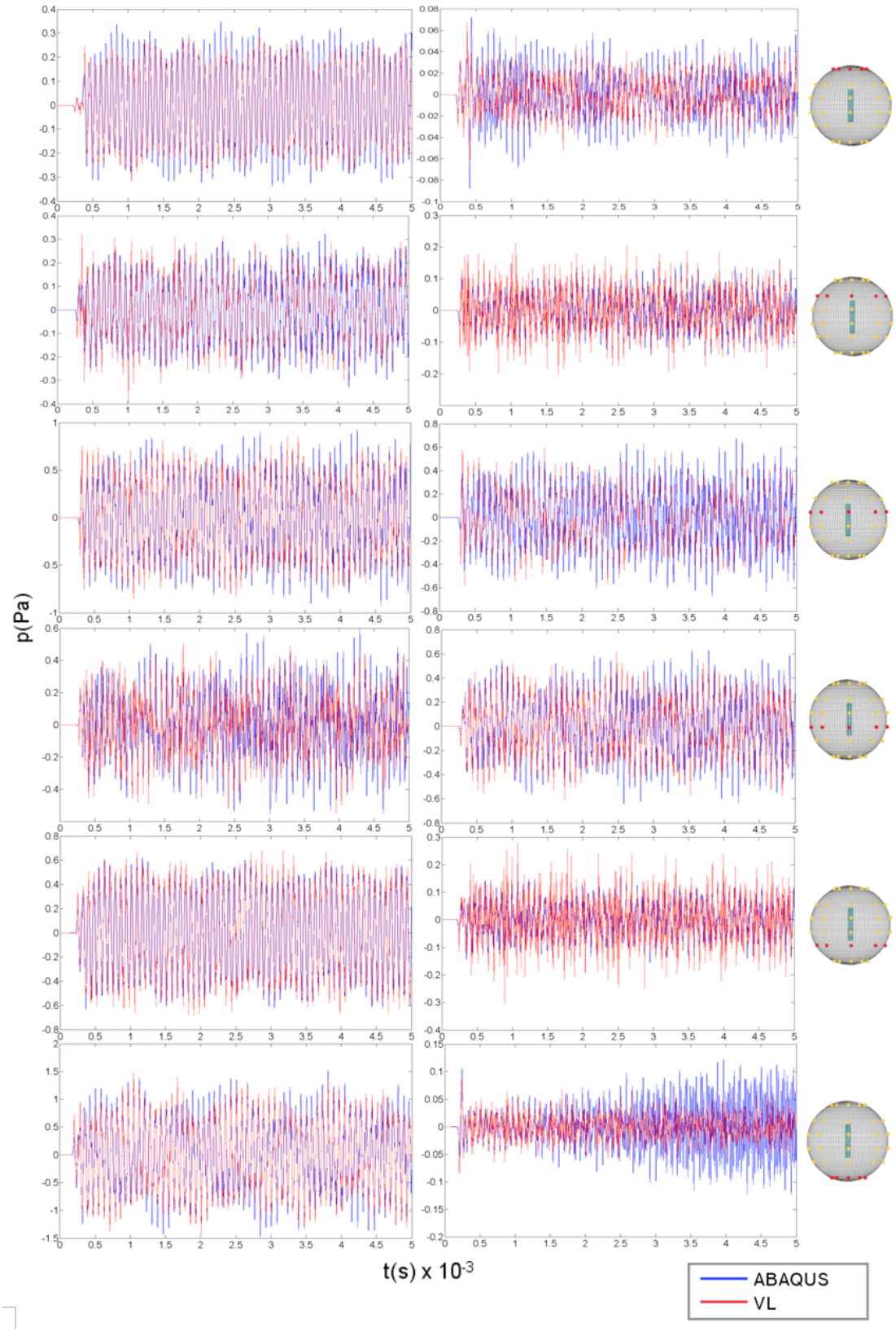

Figure 4.5.: Comparison of acoustic pressures obtained in BEM and FEM for the case including the bottom radiation (left) and the case neglecting the bottom radiation (right)

4.2. Impacted tube

4.2.1. Acoustic Pressures

For the second example, the acoustic pressures obtained for both radiation cases and methods in some microphones are shown in Figure 4.5. The red curve display the Virtual.Lab results while the blue one represent the ABAQUS results.

For the case with the bottom radiation, the results exhibit a good similarity in both methods.

Comparing the case where the bottom radiation is included to the one where this is neglected, we can observe for the latter that in Virtual.Lab we obtain in general higher values than the ones obtained in ABAQUS. Therefore the "untie" action, i.e. neglecting the contribution of a surface in VL is not working as effective as in ABAQUS.

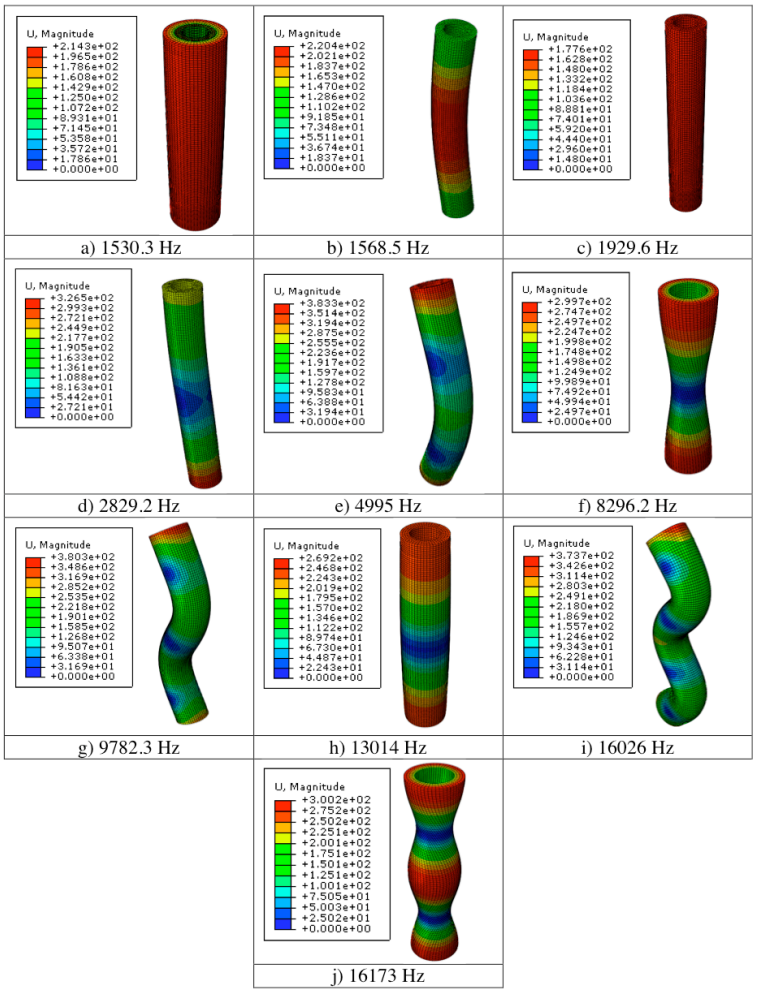

Figure 4.6.: Vibrational modes of the tube restricted with two O-rings.

4.2.2. Modal analysis

The natural frequencies and natural modes of vibrations of the tube restricted with the two O-Rings are listed in Figure 4.6. This is chief information for the late acoustic analysis because according to the case, some modes should be able to be mapped into the sound power level plot and the radiation efficiency plot. The first 6 rigid modes are captured in the subfigures **a) - d)**. Subfigure **a)** is a rotational rigid mode around y-axis; **b)** depicts 2 orthogonal modes for x- and z- axis; **c)** a translational mode in y-axis and **d)** again 2 orthogonal modes.

4.2.3. Sound Power Level

The sound power level for the fully coupled system in both cases (including or excluding the bottom surface radiation) can be seen in Figure 4.7. This fully coupled analysis was computed with the values obtained in ABAQUS. The vibrational modes at 1929.6 Hz, 2829.2 Hz, 4995 Hz, 9782.3 Hz, 13014 Hz and 16026 Hz match with the peaks of the fully coupled system without the radiation of the bottom surface. On the other hand, the blue curve only shows the vibrational mode at 1929.6 Hz. The other peaks in the curve depict spurious modes, i.e. non-physical modes.

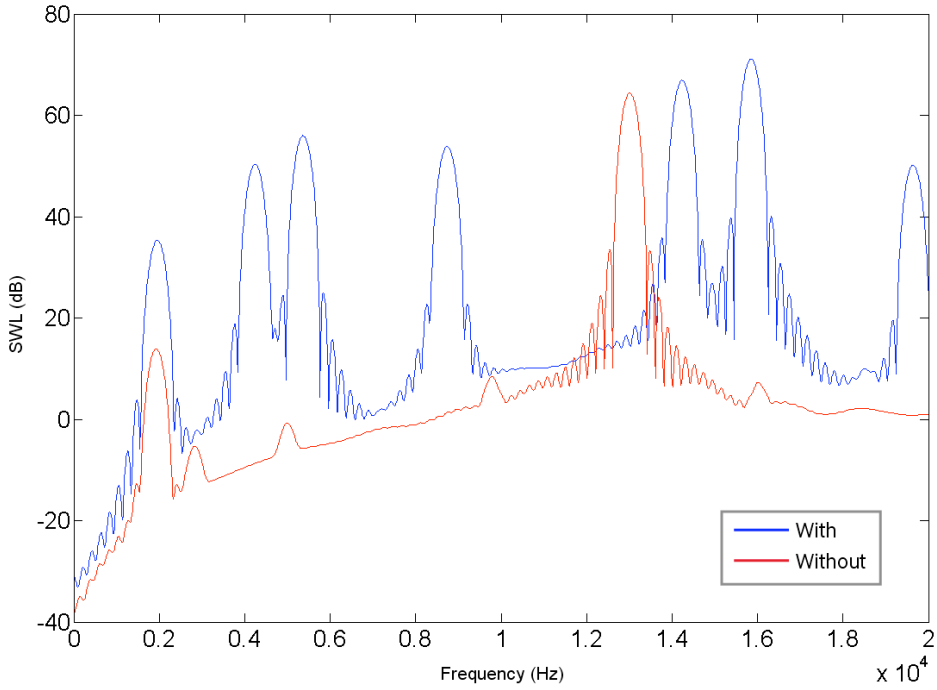

Figure 4.7.: Sound Power Level of the fully coupled system for both cases in ABAQUS

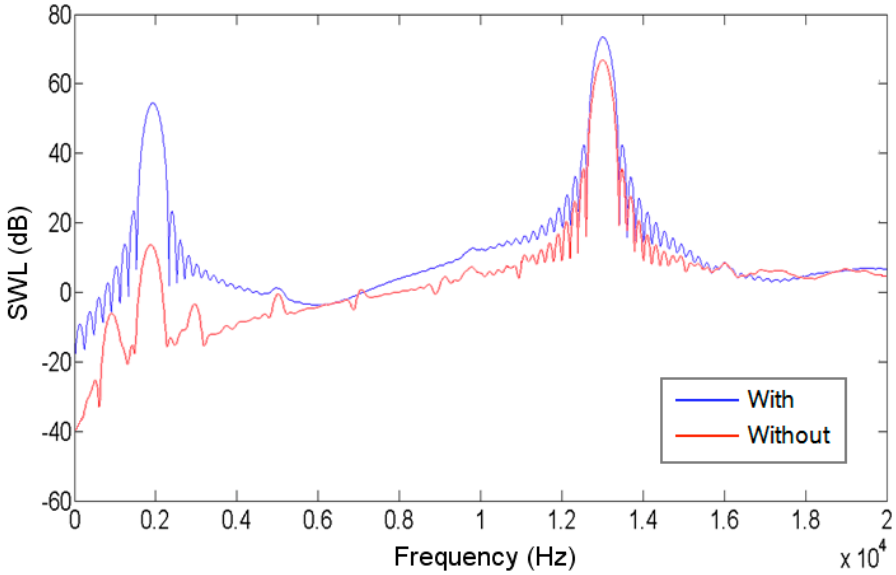

Figure 4.8.: Sound Power Level of the sequentially coupled system for both cases in ABAQUS

In Figure 4.8, since the sphere impacts on the center of the surface, the vibrational modes in y-axis should have the main influence on the sound power level. This behavior can be seen in Figure 4.8 for both cases where the other modes of vibration have almost no effect on the sound radiation. Comparing Figures 4.7 and 4.8, it can be concluded that the best workaround in ABAQUS to avoid spurious modes in this type of problem would be the implementation of a sequentially coupled system.

For the case of the sequentially coupled system, both numerical methods results were used to compute the sound power level. First, we have the system including the bottom radiation (see Figure 4.9). For this case, we can see that the values corresponding to the predominant vibrational modes match accurately for both methods.

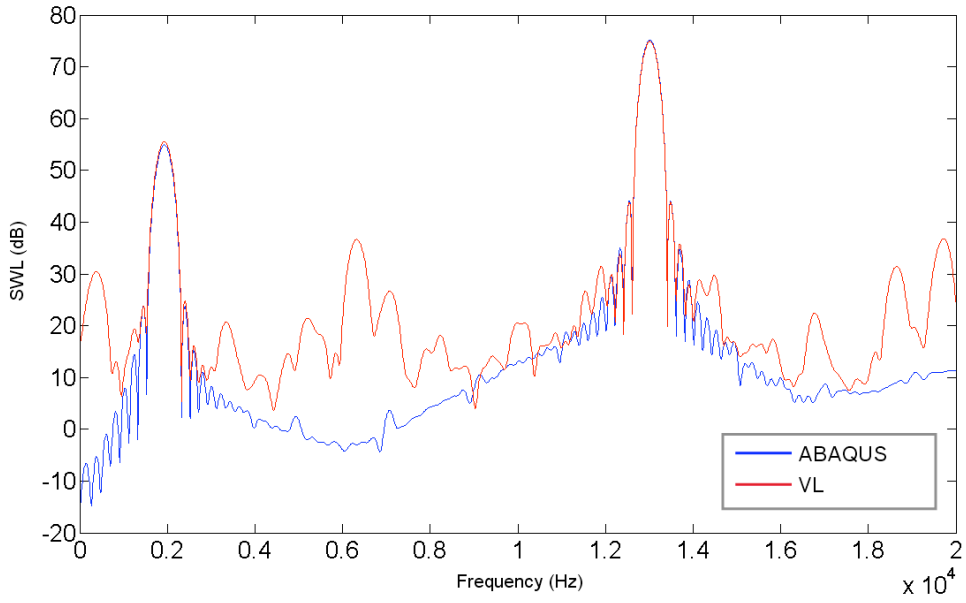

Figure 4.9.: Sound Power level of the sequentially coupled system including bottom surface radiation in BEM and FEM

When neglecting the bottom surface radiation (see Figure 4.10), we can observe that the same vibrational modes match with a little difference in the first mode at 1929.6 Hz. The sound power level computed with the values in VL are higher than the ones in ABAQUS. This was expected because of the already discussed acoustic pressure results.

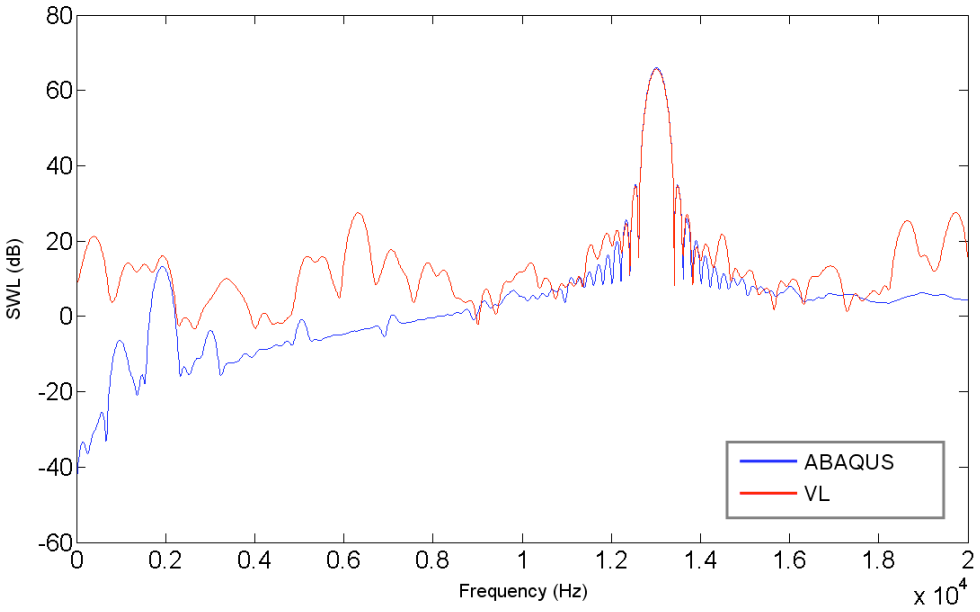

Figure 4.10.: Sound Power level of the sequentially coupled system neglecting bottom surface radiation in BEM and FEM

4.2.4. Structure-borne sound power level

In this example, since we divide the surfaces of the tube according to their relevance to the sound radiation, a simple study was performed to visualize the effect of the inclusion or exclusion of a vibrating surface in the computation of the structure-borne sound power level. In this way, the structure-borne sound power level and the radiation efficiency of the tube was computed two times starting from the values obtained in ABAQUS for the sequentially coupled system with radiation from the bottom surface.

For the *first case*, the structure-borne sound power level (3.1) was computed without taking into account the contributions of the bottom surface velocities.

For the *second case*, the same procedure was performed but the velocities on the bottom surface were considered for the computation of the structure-borne sound power level.

Finally, the radiation efficiency was computed with the two structure-borne sound power values.

The results of the structure borne-sound power level for both cases can be seen in Figure 4.11. The two dotted vertical lines represent the frequencies at which the main differences are appreciated and happen to coincide also with the frequencies at which the two modes of vibration **(c)**$1929.6Hz$ and **(h)**$13014Hz$ occur (see Figure 4.6). These modes are the ones that mainly contribute to the vibration of this surface because they are translational modes in the y-direction, i.e. the normal direction to the surface.

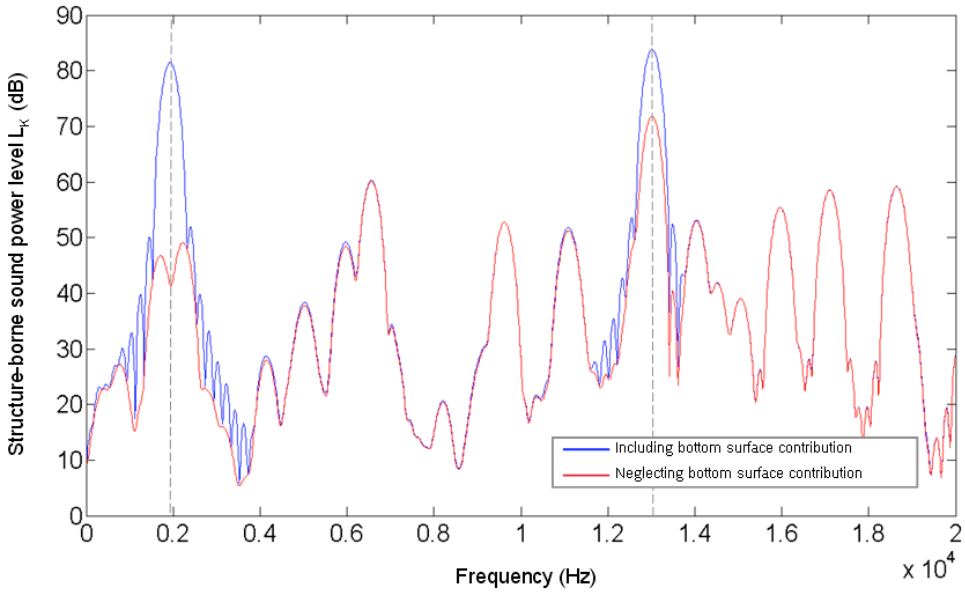

Figure 4.11.: Structure-borne sound power level of the sequentially coupled system with bottom radiation in ABAQUS

The radiation efficiency is shown in Figure 4.12. As in the previous figure the two dotted lines represent the same vibrational modes.

The contribution of the radiating surfaces for the computation of the structure-borne sound power level is very important as we can observe. When the velocities of the bottom surface are neglected, the radiation efficiency values are greatly overestimated at the frequencies where this surface is mainly excited.

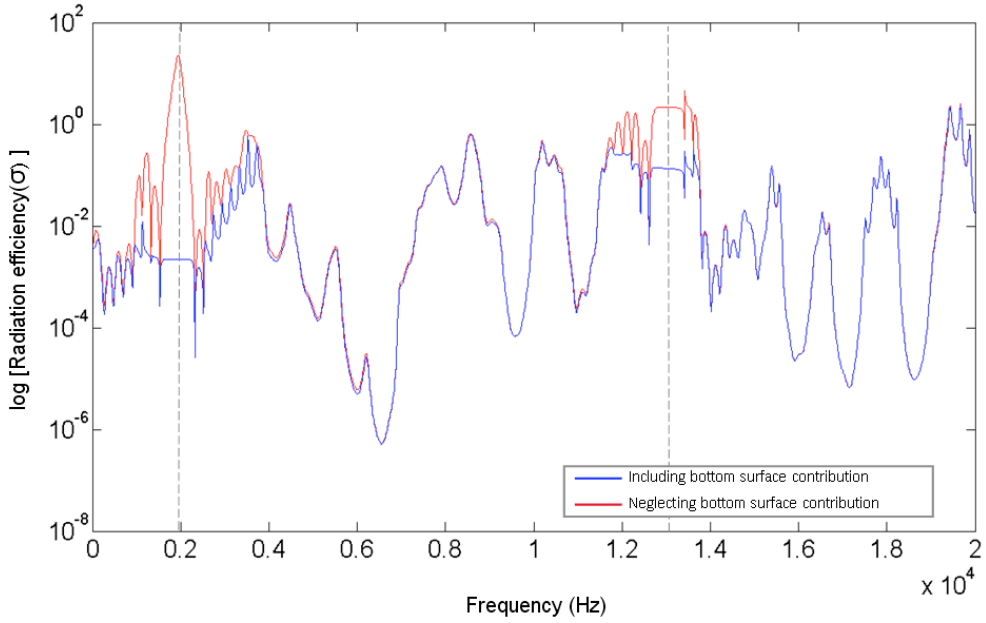

Figure 4.12.: Radiation efficiency of the sequentially coupled system with bottom radiation in ABAQUS

A similar study was performed for the fully coupled system in both cases, and the results are summarized in the Appendix (Figures A.1 and A.2). The same pattern can be seen in these results.

Taking these effects into account, the final results of the structure-borne sound power level for our fully- and sequentially coupled systems for both cases are shown in the appendix.

4.2.5. Radiation efficiency

The radiation efficiency is computed for both cases and methods as well. First, we have the radiation efficiency of the sequentially coupled surface with bottom radiation (see Figure 4.13). It is observed that the BE results show good agreement with the FE results.

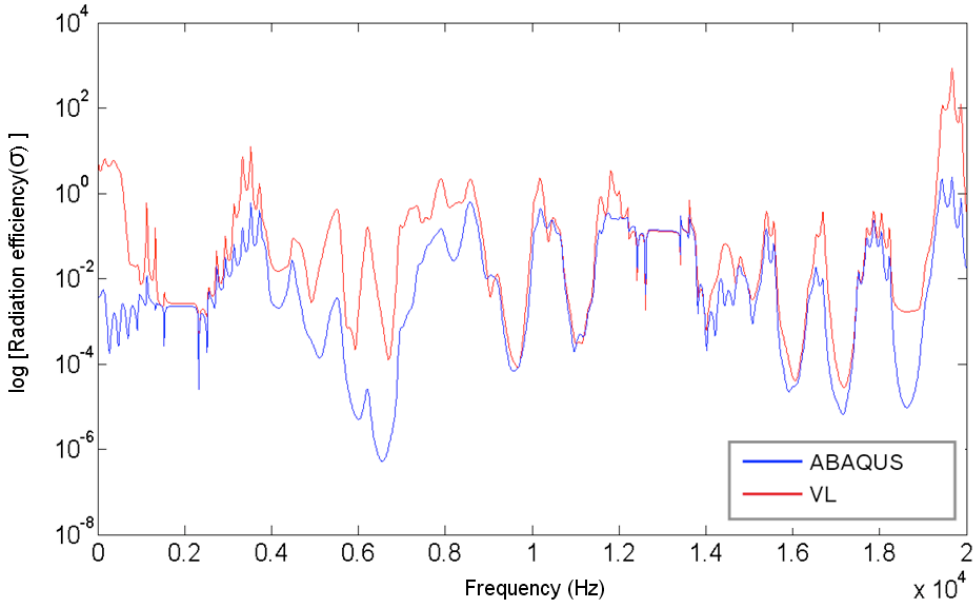

Figure 4.13.: Radiation level of the sequentially coupled system considering bottom surface radiation in BEM and FEM

For the other case, where the bottom radiation is neglected (see Figure 4.14), the results differ, in particular for the first mode of vibration. Apart from that, the corelation is as good as for the first case.

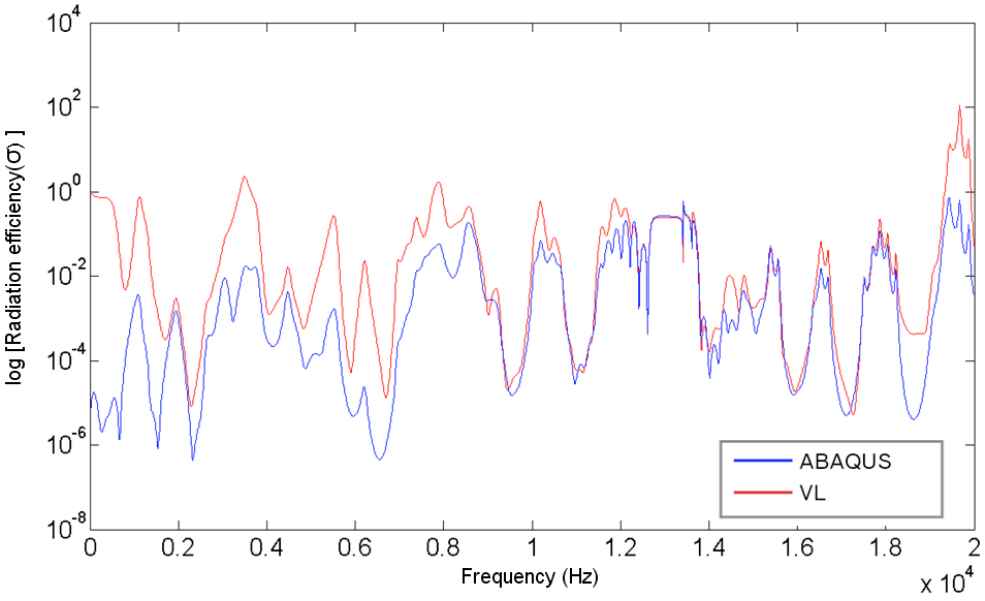

Figure 4.14.: Radiation efficiency of the sequentially coupled system neglecting bottom surface radiation in BEM and FEM

4.2.6. Time Comparison

The time for the submodel simulation in the sequentially coupled system was measured and compared between both methods. The simulation in VL is approximately 3000 times faster than the simulation in ABAQUS. The number of processors was already taken into account for this computation since the simulations were run on different computers.

The modeling time in VL for the same sequentially coupled system can be estimated as approximately the same amount of time that it takes in ABAQUS to model the acoustic medium and set the appropriate boundary conditions for the submodeling case. For the two examples, the modeling for VL was performed relatively fast since we were working with simple structures. Therefore there was no need to cover holes, eliminate unnecessary ribs or neglect fillets. These properties of the structure may be considered or not depending on the frequencies of study and the relative size of these ones to the whole structure.

5. Concluding Remarks

Considering the results discussed in the previous chapter an evaluation of the performance of Virtual.Lab in time domain IBEM can be summarized as follows.

The acoustic pressure results for both examples showed similar behavior in general. Some discrepancies were found when trying to reproduce the untie effect of ABAQUS in Virtual.Lab but on the other hand, the response in front of an abrupt signal is better than the response obtained in ABAQUS.

The accuracy on Virtual.Lab is not as good as the one obtained for FEM in ABAQUS. The relative error of the pressure values that could be computed for the case of the monopole showed that in Virtual.Lab an error of approx 6% was maintained along the frequency range. On the other hand, in ABAQUS, the error percentage obtained was definitively lower with oscillating values.

Regarding the time consumption: The FEM is a tool that demands a considered amount of time for acoustic exterior problems since the values in each node of the acoustic domain have to be computed. The BEM has a big advantage over the FEM in this field as it could be demonstrated by the pre-processing and simulation time measured for these examples.

This investigation compares the results theoretically. In order to perform a better evaluation of the software some recommendations can be made. To perform a more practical example and compare the results with values measured in an experiment could bring some more information about the performance of this tool. Another recommendation can be to reproduce the exclusion of the surface contribution to the radiation by means of another approach such as including surfaces with absorbing properties or as choosing as a target mesh only the surfaces we want to include and obtaining an open acoustic mesh which would not be an issue since the time domain module works with the indirect BEM approach.

Depending on its use, Virtual.Lab could be a very powerful tool that has to be used considering its advantages and disadvantages. The BEM approach for the acoustic problems could give accurate enough results to predict the behavior of a system thanks to the inexpensive way that the computation and visualization of the solution in an exterior acoustic problem is performed.

A. Appendix

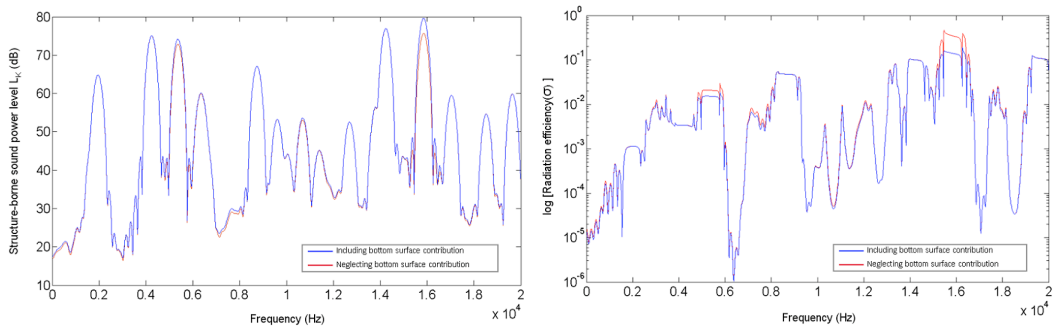

(a) (b)

Figure A.1.: Structure-borne sound power level (a) and radiation efficiency (b) for the fully coupled system including and excluding the contribution of the velocities on the bottom surface for the case in which the bottom radiation is included

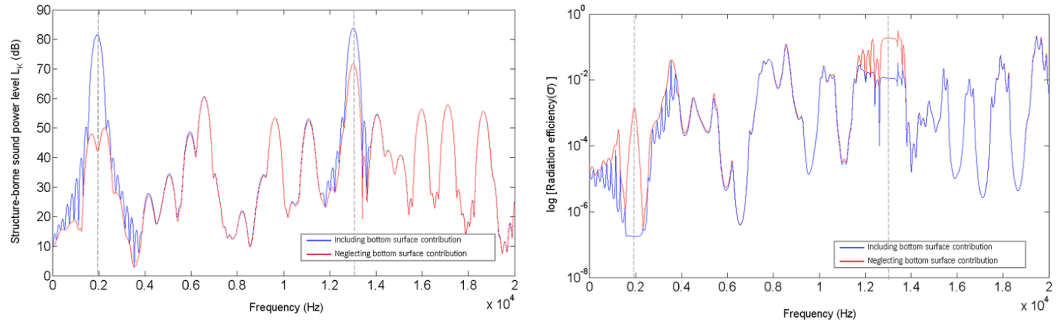

(a) (b)

Figure A.2.: Structure-borne sound power level (a) and radiation efficiency (b) for the fully coupled system including and excluding the contribution of the velocities on the bottom surface for the case in which the bottom radiation is excluded

,

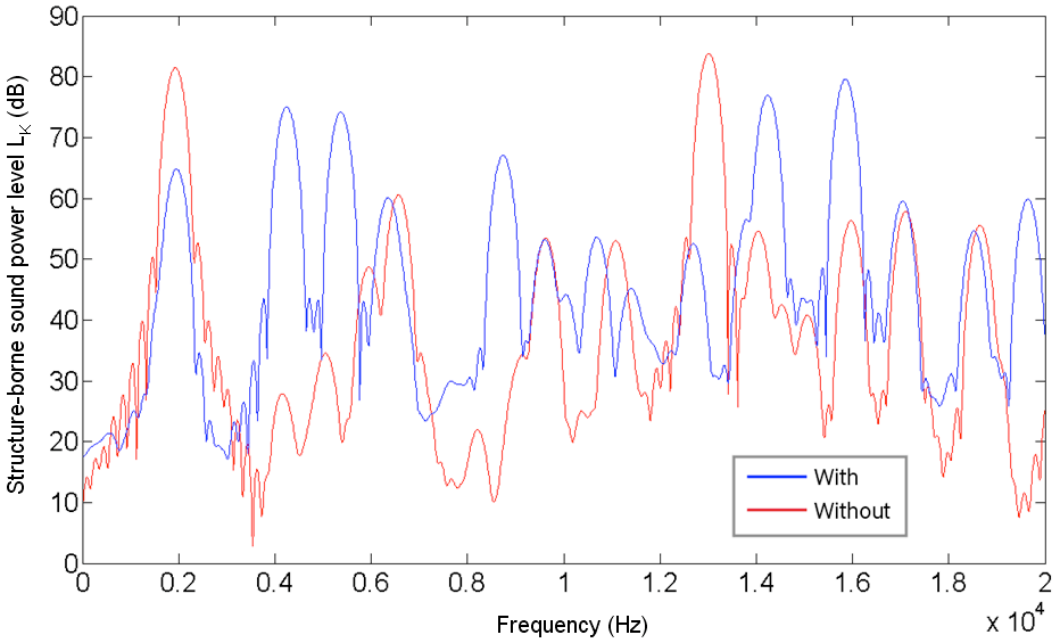

Figure A.3.: Structure-borne sound power level for the fully coupled system considering both cases

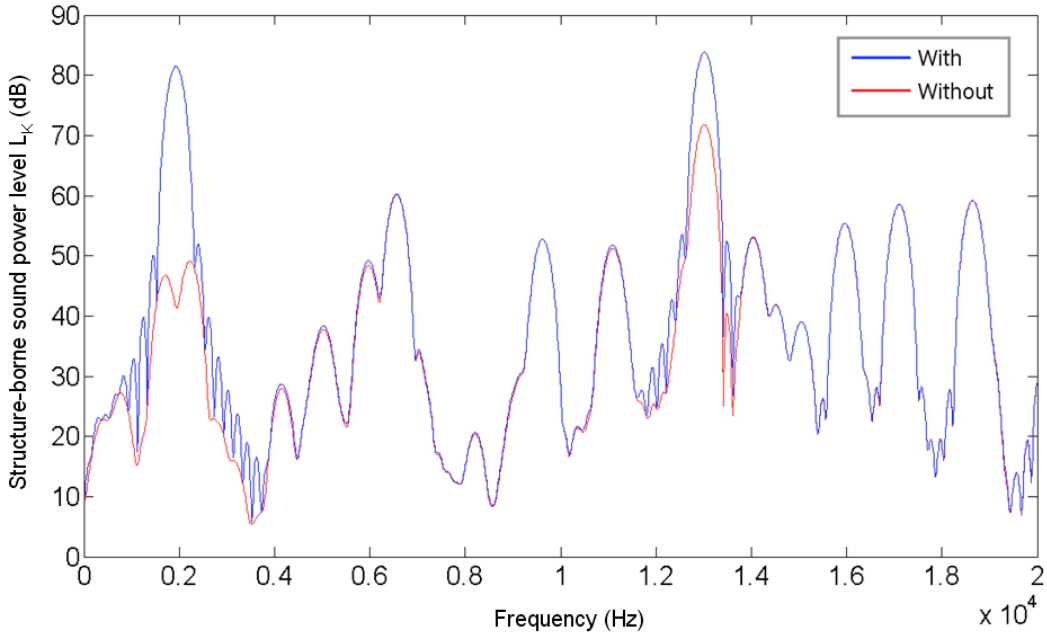

Figure A.4.: Structure-borne sound power level for the sequentially coupled system considering both cases

Bibliography

[1] *ABAQUS Theory Manual.* Dassault Systèmes, 2010

[2] *LMS Virtual.Lab. User's Manual.* LMS International, 2010

[3] Broch, J. T.: *Mechanical Vibration and Shock Measurements.* First edition. Brüel & Kjaer, 1991

[4] Fahy, F. ; Walker, J.: *Fundamentals of noise and vibration.* First edition. Spon Press, 1998

[5] Gaul, L. ; Kögl, M. ; Wagner, M.: *Boundary Element Methods for Engineers and Scientists.* First edition. Springer, 2003

[6] Henn, H. ; Sinambari, G. R. ; Fallen, M.: *Ingenieurakustik.* Fourth edition. Vieweg + Teubner, 1999

[7] Kollmann, F.G.: *Maschinenakustik.* Second edition. Springer, 2000